INVESTIGATING THE GENETIC MAKEUP AND VULNERABILITIES IN CLEAR CELL RENAL CELL CARCINOMA

Aleisha Monique Smith

A dissertation submitted to the faculty at the University of North Carolina at Chapel Hill in partial fulfillment of the requirements for the degree of Doctor of Philosophy in the Curriculum of Genetics and Molecular Biology.

Chapel Hill
2019

Approved by:

William Kim

Albert Baldwin

Yuliya Pylayeva-Gupta

Bernard Weissman

Qing Zhang

ABSTRACT

Aleisha Monique Smith: Investigating the genetic makeup and vulnerabilities in clear cell renal cell carcinoma
(Under the direction of William Kim)

Hypoxia inducible factors (HIFs) are well characterized to being functionally distinct in their transcriptional activity as well as exerting opposing effects on other transcription factors, notably c-MYC. While evidence has shown HIF1α inhibits while HIF2α promotes MYC activity, such efforts were not done within the context of ccRCC. Here we describe our efforts to investigate MYC activity in the presence of HIF2α (H2) or HIF1α and HIF2α (H1H2). While we confirmed HIF2α cells show elevated cell cycle promoting genes, such results did not correlate to any observable genome-wide significant difference in MYC dependent genes.

Renal carcinoma is a common and aggressive malignancy whose histopathogenesis is incompletely understood and that is largely resistant to cytotoxic chemotherapy. We present two mouse models of kidney cancer that recapitulate the genomic alterations found in human papillary (pRCC) and clear cell RCC (ccRCC), the most common RCC subtypes. MYC activation results in highly penetrant pRCC tumours (*MYC*), while MYC activation, when combined with Vhl and Cdkn2a (Ink4a/Arf) deletion (*VIM*), produce kidney tumours that approximate human ccRCC. RNAseq of the mouse tumours demonstrate that *MYC* tumours resemble Type 2 pRCC, which are known to harbour MYC activation. Furthermore, *VIM* tumours more closely simulate human ccRCC. Based on their high penetrance, short latency, and histologic fidelity, these models of

papillary and clear cell RCC should be significant contributions to the field of kidney cancer research.

To my family

ACKNOWLEDGEMENTS

Sean Bailey generated the various cohorts of GEM mice before my time in the lab and was instrumental in mentoring me when I first joined the lab. Jordan Kardos was instrumental in performing the bioinformatics related to analysis of the RNA-seq data associated with the GEMM data. Mi Zhou was also instrumental in performing the preliminary RNA-seq analysis of the H1H2 vs H2 project.

Much appreciation and gratitude to my advisor, William Kim for being a constant source of encouragement and compassion. I thank all members of the Kim lab for providing meaningful conversation, help with countless experiments, as well as thoughtful and useful feedback during this process.

Thank you to all members of my committee for fostering an environment in which I could openly discuss my shortcomings and problems as well as providing valuable critiques and suggestions.

TABLE OF CONTENTS

LIST OF TABLES

LIST OF FIGURES

CHAPTER 1: INTRODUCTION

Renal cell carcinoma exists as several histological subtypes

Renal cell carcinoma (RCC) ranks among the ten most common cancers in the United States with an estimated 73,820 new cases and 14,770 deaths to occur in 2019[1]. RCC is a heterogeneous disease with several histological subtypes that possess distinct genetic alterations and clinical outcomes. The major histological subtypes (with ≥ 5% incidence) include clear cell RCC (ccRCC), papillary RCC (pRCC), and chromophobe RCC (chRCC)[2]. The remaining subtypes are very rare, each with ≤ 1% total incidence, and they include MiT family translocation, collecting duct (cdRCC), medullary, and clear cell papillary RCC as well tumors considered to be unclassified if they do not fit into any the categories listed.

Clear cell RCC tumors are the most prevalent and malignant subtype of RCC and make up approximately 75% of RCC tumors[2]. These tumors derive their name from the 'clear' appearance of lipid laden cells—making ccRCC histologically distinct from the other subtypes. ccRCC tumors are further characterized by the biallelic loss of the von Hippel-Lindau (*VHL*) tumor suppressor gene, which encodes the protein VHL (pVHL)—the substrate recognition component of the E3 ubiquitin ligase that degrades hypoxia-inducible factors (HIFs). Loss or inactivation of *VHL* leads to aberrant accumulation of HIFs—resulting in uncontrolled activation of HIF target genes that regulate angiogenesis, glycolysis, and apoptosis.[3] In addition to VHL loss, recent genomic

studies have discovered additional significantly mutated genes in ccRCC such as those involved in chromatin remodeling: *SETD2*, *BAP1*, and *PBRM1*[4–6]. These genes, including VHL, make up the characteristic deletion of chromosome 3p unique to ccRCC.

Papillary RCC tumors make up approximately 10-15% of RCC tumors and is histologically characterized by the arrangement of tumor cells in a papillary configuration with fibrovascular cores. pRCC is further subclassified into two subtypes—pRCC Type 1 and pRCC Type 2[2]. pRCC Type 1 tumors make up the majority of papillary RCC tumors (approximately 60-70%) and are associated with activation of the mesenchymal-epithelial transition factor (*MET)*[7] proto-oncogene whereas pRCC Type 2 tumors (making up approximately 30-40% of pRCC tumors) have been shown to be associated with activation of *MYC*, also a proto-oncogene[8].

Chromophobe RCC (ChRCC) makes up approximately 5% of all RCC tumors. Although ChRCC is considered quite indolent compared to ccRCC tumors, with greater than 90% 10 year cancer-specific survival, aggressive features and metastasis can occur. ChRCC is defined by two histologic categories, “classic” and “eosinophilic”. Classic ChRCC demonstrate classical pale cytoplasmic features for which the disease is named while eosinophilic is defined based on abundant, eosinophilic cytoplasm and densely packed mitochondria.[9] Furthermore, ChRCC is associated with germline mutation of folliculin (*FLCN)* in the autosomal-dominant cancer predisposition Birt-Hogg Dube` (BHD) syndrome[10], as well as germline mutation of PTEN in Cowden syndrome.[11]

New methodologies such as next generation sequencing has made it possible to develop a deeper understanding to the underlying genetic alterations responsible for the

tumorigenesis of RCC. Such revelations have warranted the need to stratify patients accordingly in an attempt to ultimately curate therapies specific to the unique genetic alterations each subtype harbors. Researchers and clinicians can better investigate the relationship between molecular elements and clinical features as well as therapeutic responses to active and new therapies.

Overview of VHL

pVHL is a component of a complex with ubiquitin ligase activity

While *VHL* constitutes the most frequent and notable sporadic mutation of ccRCC tumors, it was first discovered within the context of VHL disease—a hereditary, autosomal-dominant disease associated with various tumor types including ccRCC tumors, central nervous system and retinal hemangioblastomas, pheochromocytomas and pancreatic neuroendocrine tumors, in addition to pancreatic and renal cysts. VHL disease was named by Eugen von Hippel for his description of retinal angiomatosis as well as Arvid Lindau for his description of cerebellar and spinal hemangioblastomas—hence von Hippel Lindau (VHL). Patients with VHL disease possess a single mutated allele and tumor development depends upon the spontaneous inactivation or loss of the second wild type allele. Early research demonstrated *VHL* as a tumor suppressor gene (TSG) from studies of loss of heterozygosity (LOH) showing that inactivation of both *VHL* alleles is a crucial event in the development of neoplasms in both VHL disease and sporadic ccRCC. In addition, biological evidence demonstrated that the re-introduction of the wild type VHL protein (pVHL) into a *VHL*-null ccRCC cell line had no significant effect on proliferation *in vitro* but pVHL did inhibit the ability of cells to form tumors *in*

vivo within nude mice.[12] Such evidence suggests that pVHL may rely upon cell-extracellular matrix interactions that cannot be adequately replicated *in vitro*.

The *VHL* gene encodes two isoforms of pVHL—a 30kDa form, $pVHL_{30}$ and a 19kDa form, $pVHL_{19}$. $pVHL_{19}$ lacks the 53 amino acid amino terminal pentameric acid repeat domain and is the dominant isoform expressed in many tissues. However, functional studies suggest that both isoforms exhibit the same effects in assays[12] and they both have tumor suppressor activity *in vivo*[13]. Early biochemical studies revealed that pVHL forms a tertiary complex with transcription elongation factors B and C (referred to as elongin B and elongin C). This complex is termed the VCB complex and is crucial for pVHL function. Furthermore, pVHL itself is comprised of the tightly coupled alpha and beta domains. The alpha domain is in direct contact with elongin C while the beta domain serves as the substrate recognition subunit of pVHL. The VCB complex nucleates a complex containing the following proteins: cullin 2 (CUL2) and the RING finger protein RBX1—forming the VCB-CR complex. Elongin B and C act as adapters that link pVHL to heterodimers of CUL2 and RBX1—thereby stabilizing pVHL with elongins B and C (Figure 1.1).

Figure 1.1 pVHL is part of the E3 ubiquitin ligase

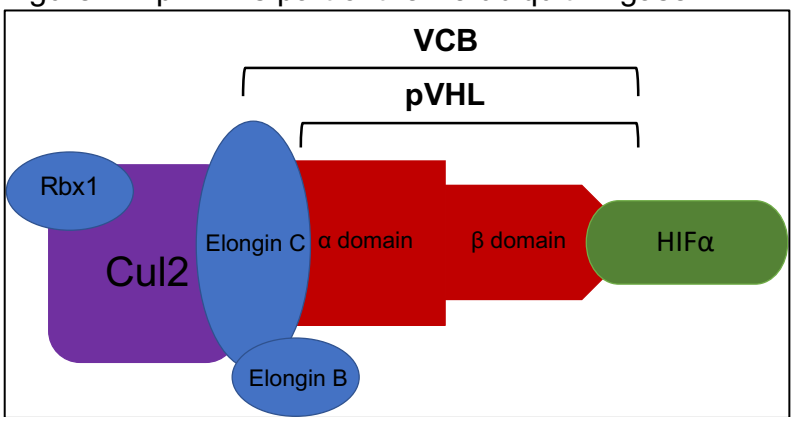

In turn, elongins B and C are also stabilized through their interactions with each other and pVHL. However, mutations in pVHL that disrupt elongin binding are unstable and are readily degraded by the proteasome. Interestingly, mutations in *TCEB1* (which encodes elongin C) affecting the ability of elongin C to bind to pVHL have been described in ccRCC[4]. Such functional and genomic studies demonstrate that *VHL* mutations relate to the dysfunction of the VCB complex and not just pVHL alone. It was noted early on that the VCB-CR complex structurally resembled that of the Skp1-Cdc53-F box protein (SCF) ubiquitin ligases in yeast. Subsequent work revealed that the VCB-CR complex also has ubiquitin ligase activity and is capable of targeting proteins for proteasomal degradation[14–17].

pVHL-HIF axis

It was noted early on that VHL disease tumors were highly vascularized and overproduced angiogenic polypeptides such as vascular endothelial growth factor (VEGF). Early biochemical studies revealed that pVHL may play a critical role in the cellular signaling generated by changes in oxygen levels when ccRCC cells lacking wild type pVHL were observed to produce high levels of VEGF, glucose transporter 1 (GLUT1), and platelet-derived growth factor subunit B (PDGFB) mRNAs regardless of

oxygen levels—that is in either normoxic or hypoxic conditions. Reintroduction of wild type pVHL inhibited the production of these mRNAs under normoxic conditions. Furthermore, Maxwell and colleagues demonstrated the crucial role for pVHL in the regulation of hypoxia-inducible factor 1α (HIF1α)[18]. Subsequent studies over the next few years elucidated the details of the pVHL-HIF pathway and the role of the VCB-CR complex in targeting HIFs for polyubiquitylation and proteasomal degradation.

The elucidation of the crystal structure of the VCB complex bound to the carboxy-terminal oxygen-dependent degradation domain of HIF1α supported evidence[17] that HIFα (both HIF1α and HIF2α) bind exclusively to the β-domain of pVHL. Such binding is dependent upon the hydroxylation of two conserved proline residues within HIF1α (P402 and P564) and HIF2α (P405 and P531) by prolyl hydroxylase (PHD) 1 (PHD1), PHD2, and PHD3. These hydroxylases require oxygen as a co-substrate (as well as iron and 2-oxoglutarate) and are thereby only active under normoxic conditions[19–21]. Prolyl-hydroxylation of HIF1α allows for its recognition and ubiquitylation by the VCB-CR complex—leading to polyubiquitylated HIFs and subsequent proteasomal degradation. During hypoxic conditions (or in the absence of functional pVHL), HIFα subunits accumulate, translocate to the nucleus, and form heterodimers with its HIFβ-subunit. These heterodimers bind to hypoxia-response elements (HREs) throughout the genome and activate genes that promote adaption to acute or chronic hypoxia. Of note, HIF1α and HIF2α subunits are constitutively transcribed through a series of signaling pathways[22]. However, they are quickly degraded under normoxic conditions and generally have a half-life of approximately five minutes[23]. This oxygen dependent

regulation of HIFα subunits is now appreciated as being a fundamental process in how cells sense oxygen (Figure 1.2).

Figure 1.2 pVHL-HIFα pathway

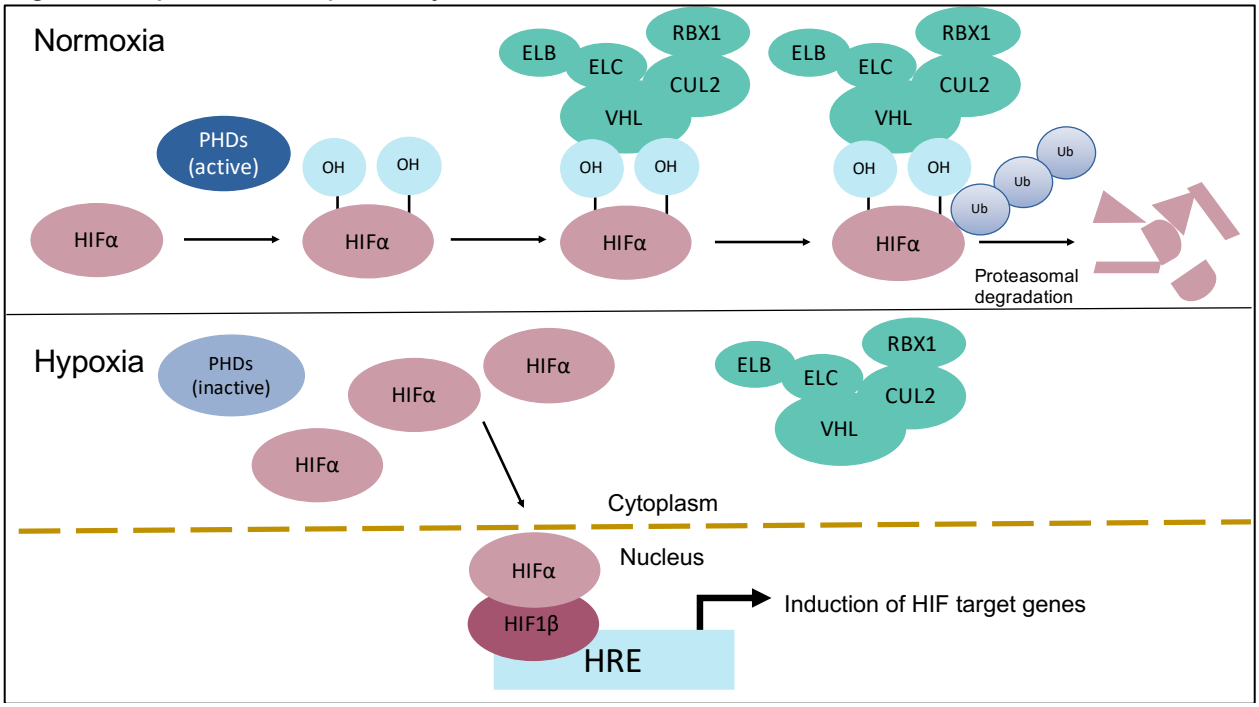

Hypoxia-inducible factors (HIFs)

Structure of HIF proteins

HIF transcription factors exist as heterodimers with an oxygen labile α-subunit (of which there are three isoforms: HIF1α, HIF2α, and HIF3α) and a stable β-subunit (HIF1β; also known as aryl hydrocarbon receptor nuclear translocator (ARNT)). Of note, HIF1β derives its name ARNT because it was identified as a heterodimeric partner of the aryl hydrocarbon receptor (AhR). AhR is a ligand-activated transcription factor that controls the expression of a diverse set of genes[24]. HIF1β binds to AhR faciliting its translocation into the nucleus[25]. These subunits belong to the bHLH-PAS protein family

because their structures are related to two nuclear proteins found in *Drosophila* (Per and Sim, PAS) which have basic-helix-loop-helix (bHLH) motif[26]. The bHLH proteins are characterized by harboring recognizable domains (b, HLH, PAS, and TAD) which can regulate their own transcription as well as the expression of other family members. The bHLH-PAS motifs are generally essential for heterodimer formation between HIFα and HIF1β subunits and binding to HRE sequences of target genes. More specifically, the base domains (b) have DNA binding properties required for HRE binding while HLH motif is where the dimerization with other proteins takes place. The PAS is the only domain conserved among all members of this protein family (HIFα, HIF1β, AhR, and PAS).

The HIFα subunits have two transactivation domains (TAD). They are the NH_2-terminal (N-TAD) and COOH-terminal (C-TAD) domains and they are both responsible for the transcriptional activity of the α-subunits[27]. C-TAD interacts with the co-activators CREB binding protein and its paralogue p300 (CBP/p300) to modulate gene expression of HIFα[28]. N-TAD is known for providing α-subunits stability and protection from degradation[29]. Furthermore, α-subunits are distinct from their β-dimeric partner in that they possess an oxygen-dependent degradation domain (ODDD) that overlaps the N-TAD in their structures. The ODDD is crucial for mediating oxygen dependent stability in that it contains specific proline residues that are hydroxylated by PHDs in normoxia[19]. It also serves as the region that is recognized by pVHL's substrate recognition, β-domain[30] (Figure 1.3).

Figure 1.3 Regulatory domains of HIFα and HIF1β subunits

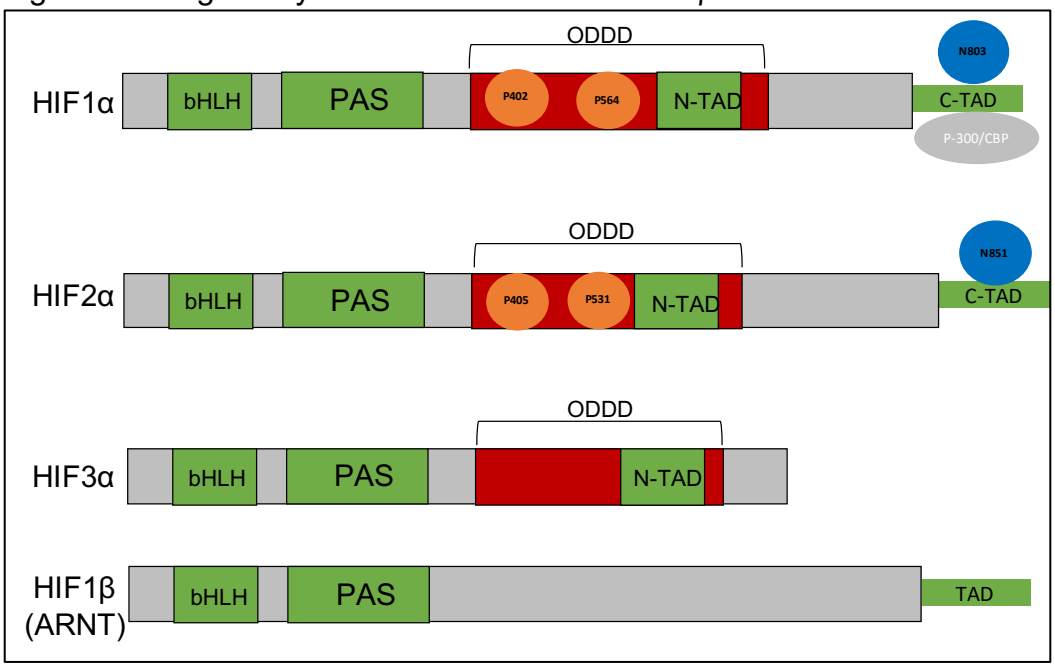

There are three HIFα subunits known to date: HIF1α, HIF2α, and the less well characterized HIF3α[27,31]. HIF1α and HIF2α share the most amino acid sequence similarity with HIF2α having 48% of sequence similarity to HIF1α. While they are similar in structure and sequence, they are expressed in different tissue patterns. HIF1α is expressed ubiquitously while HIF2α expression is limited to the kidney, heart, endothelium, small intestine, and lungs[31,32]. Although less is known about HIF3α, researchers have found that *HIF3α* gives rise to multiple HIF3α variants [22]. These variants are quite varied in that they are expressed in different tissue patterns, at different developmental stages, and are even differentially regulated by hypoxia and other factors. Evidence suggests that some variants act as dominant-negative regulators of HIF1/2α while other variants inhibit HIF1/2α activity by outcompeting HIF1β[33].

HIF1α and HIF2α (collectively referred to as HIFs) are stabilized in hypoxic conditions or when *VHL* is inactivated—as is the in case in ccRCC. However, extensive evidence has revealed that HIF1α and HIF2α are not fully redundant in function or target gene expression.

HIF1α and HIF2α transactivation domains

Early mouse studies indicated that HIF1α and HIF2α possess some unique characteristics. Targeted deletions of each isoform resulted in embryonic lethality, however the phenotypes were different. HIF1$\alpha^{-/-}$ embryos were observed to have severe blood vessel defects and died by E11[34]. HIF2$\alpha^{-/-}$ embryos were observed to have severe blood vessel defects in addition to bradycardia and abnormal lung maturation with death occurring by E13.5[35].

While HIF1α and HIF2α do harbor the same regulatory domains, variability between them is observed mostly within the N-TAD. Specifically, evidence has shown that it is the N-TAD that confers target gene specificity of HIF1α and HIF2α[36]. The C-TAD is homologous between both isoforms and promotes the expression of their common target genes[36]. As such, HIF1α preferentially activates genes involved in glycolysis such as phosphoglycerate kinase (PGK) and lactate dehydrogenase (LDH)[37,38]. HIF2α activates genes involved in tumor growth, stem cell pluripotency, and cell cycle progression such as Oct-4 and Cyclin D1[39,40]. As previously described, the hydroxylation of specific proline residues contributes to a mechanism of HIFα stability. However, another mechanism of HIFα regulation depends upon the hydroxylation of a conserved asparagine residue (N803 in HIF1α and N851 in HIF2α) located in the C-TAD by the asparaginyl hydroxylase, factor inhibiting HIF (FIH-1). Like the PHDs, FIH-1

requires iron and α-ketoglutarate[41]. FIH-1 prevents the interaction between the C-TAD and the essential co-activators CBP/p300—rendering the C-TAD nonfunctional and directly inhibiting the transcription of C-TAD dependent genes[41]. Subsequent research has suggested that HIF2α is more resistant to FIH-1 inhibition than HIF1α. This may be due to the differences of the surrounding amino acids within the respective C-TAD[42].

HIF independent functions of pVHL

pVHL's role in apoptosis

While pVHL was first characterized through its interaction with HIFα subunits, growing evidence has emerged suggesting that pVHL plays a role in regulating cellular processes independent of HIFs. ccRCC tumors are known for their resistance to conventional cytotoxic chemotherapies and such efficacy of chemotherapy is closely associated to p53-mediated apoptosis[43]. However, most ccRCC tumors do not harbor p53 mutations or loss suggesting either activation of alternative anti-apoptotic pathways or functional modulation of p53 activity[43]. Previous studies have shown that HIF can directly bind to and modulate p53 activity[44–46]. Additionally, pVHL is able to stabilize p53 in a HIF-independent manner by suppressing MDM2-medidated ubiquitination and nuclear export resulting in increased transcriptional activity[47].

Genetically engineered mouse models (GEMMs) of RCC

Inactivation of Vhl in murine kidneys does not recapitulate human RCC

Accumulating knowledge on the underlying biology of RCC has led to the development of targeted therapy blocking the von Hippel Lindau (VHL)-hypoxia inducible factor (HIF) pathway and its gene products or the mTOR pathway[48]—leading to improved clinical outcomes. However, it remains that a subset of patients are

intrinsically refractory to such targeted therapies and most patients exhibit tumor regression only during the first few months of treatment. Drug resistance typically occurs after a median of 6 to 15 months of treatment, leading to cancer progression and eventual death[49]. A recent resurgence of immunotherapy has shown great promise for patients with advanced RCC who are refractory to other treatments[50]. The role of these emerging treatments for the management of metastatic RCC still needs to be established with ongoing trials along with the opportunities to perform precision based medicine. Such efforts call for the generation of preclinical animal models. Genetically engineered mouse models (GEMMs) serve as powerful tools to explore the tumorigenesis of a wide variety of cancers as well as indispensable preclinical models for drug testing. While ccRCC is among one of the few cancers known to evolve from a specific genetic mutation, mouse models that recapitulate its characteristic molecular and cellular features have not generated the expected outcome. Fortunately, extraordinary efforts have been made within the past few years to take on the challenge of developing mouse models of ccRCC that are faithful to the human disease.

As described above, VHL inactivation has been shown to occur in approximately 92% of sporadic ccRCCs[4]. The role of VHL as a tumor suppressor in cancer has been established by the fact that reintroducing wild type *VHL* into *VHL* null RCC cell lines disrupts their capacity to form tumors in immune-comprised mice[12,51]. However, early efforts have revealed that inactivation of VHL within kidney cells do not transform cells or produce RCC within mice. Homozygous germline deletion of *Vhl* in mice led to embryonic lethality[52]. Furthermore, a mosaic deletion[53] or heterozygous deletion of *Vhl*[54,55] does not predispose mice to RCC—in contrast to what occurs in humans[56].

Subsequent efforts have focused on generating models that utilize the Cre-Lox system to control spatiotemporal mutations of genes shown to be involved in the tumorigenesis of RCC.

The proximal tubular epithelial cells are generally believed to be the cell of origin of RCC and have been the first targets for conditionally targeting cells in the kidney. Specifically, Rankin and colleagues developed the first conditional knockout mouse model using the phosphoenolpyruvate carboxykinase (PEPCK)-Cre system to delete *Vhl* in renal proximal tubule cells. While they did observe cellular proliferation, lipid accumulation, and macroscopic renal cysts in 18% of mice over a year old, no RCC development was observed before mice reached 25 months[57]. Because accumulated evidence has indicated that ccRCC can at least partially originate from non-proximal tubules, such as the distal convoluted tubules and collecting ducts[58], some researchers have attempted to target non-proximal tubule cells of the kidney.

Frew and colleagues generated a conditional *Vhl* knockout mouse within the distal tubules and collecting ducts using the Ksp1.3-Cre system (which is also expressed in proximal tubules) and found no abnormalities other than hydronephrosis[59]. Another mouse model was generated by using Hoxb7-Cre to inactivate *Vhl* in the collecting ducts and a subset of distal tubules within the kidney. Mice exhibited hyperplasia, presence of clear cells and cysts, and disrupted structures—but no development of ccRCC[60]. Such efforts have revealed that VHL loss alone is insufficient for tumorigenesis within the mouse kidney. It is generally accepted that additional mutations in other tumor suppressors or oncogenes are required to initiate tumorigenesis. In accordance with this hypothesis, researchers have combined deletion

of VHL with the deletion or activation of other tumor suppressors and oncogenes, respectively, in efforts to promote ccRCC development.

Inactivation of Vhl and PTEN

The inability to produce ccRCC in mice by only inactivating *Vhl* supports the idea of combining additional genetic mutations to recapitulate the tumorigenesis of ccRCC. Large-scale genomic studies have revealed recurrent altered genes and pathways other than VHL inactivation. These genes and pathways may function cooperatively with the VHL pathway (as described above) and serve as good candidates to be investigated in ccRCC GEM models.

The involvement of phosphatase and tensin homolog (PTEN) and the PI3K/AKT pathway within ccRCC was established in early research by Velickovic and colleagues[61] and has been reconfirmed by recent genomic studies that approximately one-fifth of patients harbor mutations in genes involved in this pathway. PTEN is one of the most frequently disturbed tumor suppressor genes in sporadic cancers and negatively regulates the PI3K/AKT pathway. The PI3K/AKT pathway plays a crucial role in the cellular metabolism, proliferation, and survival[62]. Based upon these facts, Frew and colleagues generated a conditional co-deletion of *Vhl* and *Pten* in mouse kidney epithelial cells using the Ksp1.3-Cre system[59]. All of these mice developed cysts lined with reduced cilia and clear cell epithelial cells within only two months of age. No overt tumors were observed due to the euthanasia of mice within 3-6 months to avoid renal failure. However, such a combination elicited cyst formation with a short latency; encouraging further investigation of other combinatorial genetic alterations.

Inactivation of Vhl and p53

The *TP53* gene is a crucial and well known tumor suppressor—encoding its product, p53. p53 has been well characterized and serves to protect cells from DNA damage and transformation. *TP53* is regarded to be quintessential in tumorigenesis due to its frequent alteration in diverse and approximately half of all cancer types[63,64]. Unlike mutations of *PTEN* that typically abolish its tumor-suppressing function, mutations of *TP53* often confer neomorphic functions that are oncogenic in nature[65]. Although *TP53* mutations occur only in a small subset of ccRCC patients (2.08%)[5], p53 pathway-regulated genes, such as *MDM2*, *CHEK2*, *ATM*, and *CDKN2A*, are functionally mutated in approximately one-fourth of patients[4,6]. Albers and colleagues set out to investigate the role of TP53 mutations in the tumorigenesis and progression of RCC. They generated a conditional co-inactivation of *Vhl* and *Trp53* in the kidney epithelium of mice using Ksp1.3-Cre. Researchers observed tumorigenesis within the urinary tract as well as renal cysts in three-fourths of mice after one year. In addition, neoplasms were observed containing cells that showed altered proliferation as well as cytoplasmic clearing but no ccRCC tumors. Furthermore, molecular investigation revealed elevated expression of MYC and target of rapamycin complex 1 (mTOR)—demonstrating that inactivation of Vhl and Trp53 induces the development of renal cysts and ultimately progression to dysplastic and malignant lesions[66].

Inactivation of Vhl and Kif3a

The primary cilium is an organelle that is microtubule-based and found in several cell types. It mostly functions as a luminal flow sensor and is involved in regulating tubular cell proliferation within the kidney[67]. As previously stated, pVHL mediates

numerous biological activities including the stabilization of the microtubule network[68] and is important for the regulation of the primary cilium[69]. The importance of the primary cilium in renal tumorigenesis and cytogenesis in conjunction with the fact that a subset of ccRCC tumors develop in a cyst-dependent manner led researchers in interrogate the effects of Vhl inactivation coupled with the specific ablation of primary cilia in the kidney. Lehmann and colleagues conditionally deleted the kinesin family member 3A (*Kif3a*) gene, which encodes a protein subunit of the kinesin-II microtubule motor complex that is essential for cilia formation, along with *Vhl*. Both mutations were carried out using the Ksp1.3-Cre system. The combined loss of *Vhl* and *Kif3a* resulted in the formation of renal cysts with a shortened latency of cyst initiation as well as increased total cystic burden and frequency in all mice[70].

Inactivation of Vhl, Trp53, and Rb1

Noteworthy efforts by Harlander and colleagues demonstrated success in developing a mouse model of ccRCC by combining deletions of Vhl, Trp53, and Rb1 in kidney epithelial cells (Ksp-Cre system)[71]. The majority of mice (more than 80%) developed an average of five tumors per mouse within 25-61 weeks of somatic mutation. Pathological examination revealed classic clear cell tumor cells, necrosis, and intratumoral hemorrhage. Immunohistochemical staining exhibited nuclear accumulation of HIF1α and HIF2α—predictive of Vhl loss. Additionally, strong immunoactivity of carbonic anhydrase IX (CAIX), a marker known to be highly expressed in RCC tumors and thought to play a role in cellular proliferation in response to hypoxic conditions was detected[72] as well as tissue markers indicative of proximal tubule cell of origin. mTORC1 activation was confirmed and RNA-seq analysis showed strong correlation in

between the global transcriptional profiles of the triple-mutant mouse tumors and human ccRCC tumors. This mouse model has been tested in preclinical therapeutic studies, with individual ccRCC mice showing varied sensitivity to sunitinib and everolimus treatment. This suggests that this model would be useful to interrogate mechanisms of drug resistance and to identify potential therapeutic biomarkers. Although the pathways regulated by these genes are frequently altered in ccRCC, albeit through different mechanisms, the inactivation of *Vhl*, *Trp53*, and *Rb1* is not common in human ccRCC and may reflect only a small subset of human ccRCCs.

Inactivation of Vhl and Bap1

As previously described, next-generation sequencing has led to the identification of additional recurrent mutations found to reside near *VHL*, on chromosome 3p. These mutations occur in chromatin remodeling genes and include *SETD2*[73], *BAP1*[74], and *PBRM1*[75]. Such efforts have offered researchers rationale to assume that these genetic alterations may function cooperatively with *VHL* inactivation to develop ccRCC.

BRCA-1 associated protein 1 (BAP1) is a nuclear-localized histone deubiquitinase that binds to the BRCA1 RING finger domain and functions are a tumor suppressor in various cancers[76,77]. Approximately 14% of ccRCC harbor sporadic loss of BAP1 and is associated with a high-grade subset of ccRCC tumors[74]. Wang and colleagues set out to investigate the effects of combined inactivation of *Vhl* and *Bap1* using the Six2-Cre system[78]. SIX Homeobox-2 (*Six2*) is expressed specifically within nephron progenitor cells of the kidney. Mice harboring loss of *Bap1* alone were moribund and died before 1 month of age. Mice deficient in *Vhl* and only one allele of *Bap1* were initially morphologically normal but displayed increasingly extensive

abnormalities in histology starting at only 1 month of age. Perhaps most notable was the observation that lesions spanned from premalignant cysts to cystic and solid RCC tumors were identified—recapitulating such manifestations seen in patients with VHL syndrome. Molecular examination revealed positive CAIX staining as well as elevated staining for phosphor-S6, a downstream target of mTORC1 activation. Such results indicate that this mouse model was able to reproduce some features of human ccRCC. It should be noted that the loss of chromosome 3p in humans can simultaneously cause both *VHL* and *BAP1* deletion, but this would not occur in mice due to the fact that *Vhl* and *Bap1* reside on different chromosomes.

Based upon the mouse model of Vhl loss and a heterozygous loss of Bap1, the same group attempted a double deletion using different Cre drivers. While the Six2-Cre model led to mice dying shortly after birth and small kidney tumors; Sglt2-Cre and Villin-Cre systems (both are expressed within the proximal convoluted tubules) failed to induce tumors. The authors found success utilizing the paired box 8 (PAX8)-Cre system[79]. PAX8 encodes a transcription factor that plays a critical role in kidney development and is expressed in the mesonephros, metanephros, nephric duct, and ureteric bud—the complete tubular system[80]. These mice, harboring homozygous deletions of *Vhl* and *Bap1,* lived to approximately three months of age. However, these mice developed small RCC tumors and cystic lesions in the kidneys—with similar morphological features of Six2-Cre derived tumors. Authors also generated mice deficient in *Vhl* and one allele of *Bap1* using PAX8-Cre system. In contrast to the double deletion, these mice had a median survival of 14.5 months; displaying cystic lesions at 10 months and tumors at 11 months of age. Both PAX8-Cre models showed elevated

expression of HIF target genes and increased mTORC1 activation—consistent with clinical features of human ccRCC with BAP1 deficiency. Of note, this study proposed evidence that the Bowman's capsule, rather than the proximal tubule, to be the cell of origin of ccRCC.

Inactivation of Vhl and Pbrm1

Genomic sequencing has identified *PBRM1* to be the second most frequently mutated gene in sporadic ccRCC[75]. *PBRM1's* product is a subunit of the SWI/SNF chromatin remodeling complex, and is located on chromosome 3p near *VHL*. Several groups have generated mouse models with *PBRM1* deletion in attempts to recapitulate human ccRCC. Nargund and colleagues investigated the role of *Pbrm1* in the tumorigenesis of ccRCC by inactivating both *Vhl* and *Pbrm1* using a Ksp-Cre system in induce the deletion of both genes at the embryonic stage[81]. These mice developed preneoplastic polycystic kidney disease at 6-9 months of age with a 30% incidence. In addition, histologic examination revealed a 50% tumor incidence at 10 months of age. Such tumors showed key features of human ccRCC, including clear cytoplasm, positive CAIX staining, and hyperactive mTORC1 signaling. In addition the origin of these tumors from proximal tubules and gene expression profile suggests the tumors resemble ccRCC rather than other types of RCC.

Another group developed a mouse model of RCC using Pax8-Cre deletion of Vhl and Pbrm1. Their results showed the majority of mice (85%) presented with bilateral, multiple, large, and homogenous tumors at only 9 months of age with 100% of mice presenting with tumors by 13 months of age. Tumor size increased with age until almost encompassing the whole kidney at 16 months of age[79].

While both studies confirmed the tumor suppressive role of *PBRM1* and that combinatorial deletion of *VHL* and *PBRM1* predisposes mice to ccRCC—the two models have contradictory conclusions in terms of mTORC1 status. The model utilizing Ksp-Cre showed elevation of mTORC1 while the Pax8-Cre system showed hypoactive mTORC1 expression. Such differences may be due to differences in cell of origin of ccRCC.

Gu and colleagues studied the simultaneous deletion of *Vhl/Pbrm1* and *Vhl/Bap1* and discovered that *Bap1* and *Pbrm1* play an important role in determining tumor grade[79] —compatible with findings that mutations of BAP1 and PBRM1 are associated with tumor grade, aggressiveness, and patient survival in human ccRCC[74,82]. This group further investigated the pathway underlying the tumor grade differences in *BAP1* and *PBRM1* deficient ccRCC. *BAP1* deficient tumors harbor activated mTORC1 (such activation of mTORC1 not observed in *PBRM1* null cRCC) which leads to a high grade and aggressive tumor. Furthermore, the loss of one copy of TSC1 in PBRM1 null ccRCC to drive activation of mTORC1 resulted in the low grade tumors to become high grade. Such distinctions are critical for clinical practice.

While the above mentioned GEM models of ccRCC are not exhaustive, they represent significant findings and efforts within the field of RCC. Some ccRCC models can mimic most of the genetic aberrations found in human ccRCC—making them valuable tools to define the casual role of genetic events in ccRCC. Most of these models reproduce precursor lesions or a few of the important phenotypes of ccRCC—signifying the difficulty in successfully developing an autochthonous ccRCC model. Such difficulty goes to the fact that outside of *VHL* inactivation, there has not been an

established set of genes that are solely responsible for developing ccRCC within mice. However, some of these models (including the *VIM* GEM model generated by our group discussed in Chapter 3) were able to fully reproduce bona fide ccRCC in adult mice. Such strides in the generation of these indispensable models provide a means to investigate the biological mechanisms underlying tumor progression as well as the heterogeneity among patients of a given therapeutic.

c-MYC: master regulator

Regulatory domains of MYC

c-MYC (MYC henceforth) encodes the MYC transcription factor and plays essential roles in cellular proliferation, growth, differentiation, and apoptosis. The Myc protein is comprised of several domains that play crucial roles in MYC activity and stability. These domains are as follows: an N-terminal transactivation domain (TAD) required for transcriptional activation, a central region, and a C-terminal domain (CTD) critical for DNA binding and protein interactions. Myc has four conserved regions known as Myc boxes (MB) that are essential various functions. The TAD, which is responsible for the assembly of transcriptional machinery, contains MBI and MBII. MBI contributes to gene activation and protein degradation, while MBII that is critical for most of Myc's functions. The central region contains MBIII and MBIV. MBIII has been implicated in transcriptional repression, apoptosis, and transformation while MBIV modulates DNA binding and shares some functions of MBIII such as apoptosis and transformation. The CTD is comprised of a basic region required for binding to E boxes (CACGTG) and a helix-loop-helix leucine zipper (HLHZip) domain that is necessary for dimerization with one of its binding partners—Max[83].

Regulation of MYC as an oncogene

MYC was first discovered as a homolog of the retroviral *v-Myc* oncogene in avian tumors[84]. Soon after, a role for MYC in driving human cancer was first identified in B-cell Burkitt's lymphoma, where MYC was found to be deregulated due to its chromosomal translocation into the immunoglobulin heavy chain locus[85,86]. MYC's transforming ability (in cooperation with activated RAS) was first demonstrated within primary rat embryo fibroblasts[87] and has since been shown to be overexpressed in over 50% of all human tumors—supporting the notion that MYC is a human oncogene.

Due to its oncogenic potential, *MYC* is tightly regulated in noncancerous cells at transcriptional and post-transcriptional levels via miRNAs and by translation of its own mRNA[88–90]. Post-translationally, MYC protein half-life and transcriptional activity are regulated by kinases, ubiquitin ligases, acetyltransferases, and other interacting proteins[83,88–92]. In support of this, evidence has demonstrated that oncogenic KRAS and ERK can upregulate MYC, in part, through enhanced protein stability[83,93–95]. Additionally, studies have shown that long noncoding RNAs (lncRNAs) control MYC protein stability and activity by altering post-translational modifications[92,96]. Many growth promoting signaling pathways, such as NOTCH and EGFR, converge on MYC—underscoring the centrality of MYC to cell growth regulation[97–103]. In stark contrast to MYC's activity within normal cells, MYC amplifications within cancers that increase copy number, translocations that pair MYC with highly active enhancers, or viral insertion events within the MYC locus abolish MYC's dependence on growth factor signaling[104]. Changes in the activity of MYC's enhancers can perturb MYC expression from its normally required stimuli, affecting cancer risk and progression. For instance, NOTCH-

dependent enhancers of MYC appear to be intimately involved in the activation of MYC in human T-cell lymphoma[105,106]. Other enhancers show single-nucleotide polymorphisms (SNPs) that affect transcriptional activator TCF-7 binding and predispose patients to colon and prostate cancers [107–109].

Gain of MYC occurs in a subset of ccRCC patients

Deregulation of MYC expression in cancers is inherently different from regulated MYC expression in normal cells. Aberrant expression of MYC is shown to induce a transcriptional response network different from the response triggered by endogenous normal MYC. Loss of function analysis of MYC reveals its crucial role in the growth of T lymphocytes, keratinocytes, and intestinal crypts[110–112]. Further proof as to the difference of MYC's transcriptional program between cancerous and normal cells is the expression of cyclin-dependent kinase inhibitors are generally elevated while expression of cyclin-dependent kinases are repressed in resting, or normal, cells. Researchers have demonstrated there are a subset of ccRCC tumors that harbor a gain of chromosome 8q (where MYC resides). Additional studies have shown ccRCC tumors with a gain of 8q24 consistently overexpressed c-MYC. Furthermore, amplification of this locus was associated with decreased DSS (disease-specific survival) as well as an increased risk of regional lymph node metastases and distant metastases. [113]

INK4a/ARF

INK4a/ARF locus

The INK4a/ARF locus (also known as CDKN2A on chromosome 9p21) encodes two structurally and functionally distinct tumor suppressors: $p16^{Ink4a}$ and $p19^{ARF}$. These proteins have different first exons that are spliced to a common second and third exon.

While exons 2 and 3 are shared between p16 and p19, the proteins are encoded in alternative reading frames—resulting in no amino acid homology between the two proteins (Figure 1.4).

Figure 1.4 INK4a/ARF locus encodes TSGs that regulate cell cycle

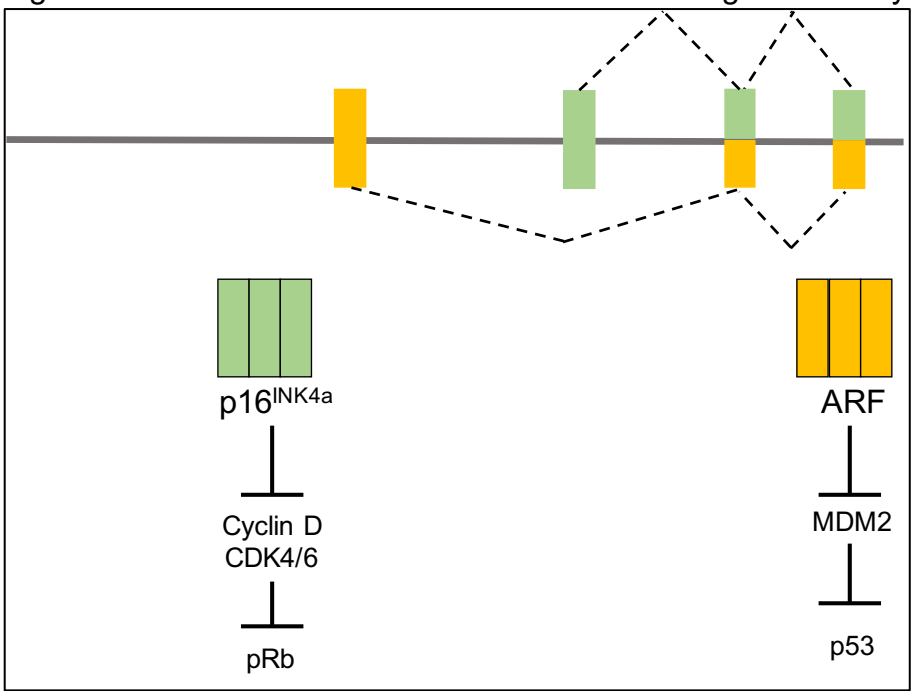

Cell cycle arrest by $p16^{Ink4a}$ and ARF

Perhaps the most well studied function shared by inhibitors of Cdk4 (Ink4a) and alternate reading frame (Arf) is their ability to cause cell cycle arrest. The tumor suppressor proteins Ink4a and Arf function in distinct pathways. Ink4a regulates the retinoblastoma (Rb) pathway while Arf regulates the p53 pathway. Upon the induction of D-type cyclins by extracellular growth factors, they associate and bind with cyclin-dependent kinases 4 and 6 (Cdk4 and Cdk6). This cyclin-Cdk complex is responsible for phosphorylating, and thereby inactivating, the retinoblastoma protein (pRb). Inactivation of pRb results in the activation of E2F-dependent transcription of genes necessary for DNA replication and S phase. Among the E2F target genes is cyclin E—

which maintains the phosphorylation of pRb in conjunction with Cdk2. Ink4a exerts its ability to halt cell cycle progression by binding directly to Cdk4 and Cdk6[114], disrupting them from associating the D type cyclins. This results in the pRb being in a 'hypo-phosphorylated' state and therefore in an active state—leading the inactivation of E2F-dependent genes. In addition to inhibiting Cdk4/6, excess Ink4a can inhibit Cdk2 (thereby disrupting the cyclin E-Cdk2 complex) by causing the redistribution of the p21 family of Cdk inhibitors from cyclin D-Cdk complexes to cyclin E-containing complexes. The net result is an arrest in the G1 phase (Figure 1.4).

Murine double minute 2 (Mdm2) is well known for being a critical modulator of p53 activity by directly promoting p53's proteasomal degradation[114]. Interestingly, Mdm2 is activated by p53—setting up a feedback loop through which p53 function is tightly controlled. Arf's ability to cause cell cycle arrest is due to its binding to Mdm2 and inhibiting its E3 ubiquitin ligase activity—resulting the stabilization of p53 and activation of its target genes (Figure 1.4). These target genes include p21, which presumably underlies Arf's ability to cause cell cycle arrest. However, several groups have shown evidence that there may be other possible mechanisms at play that allow Arf to cause cell cycle arrest. It has been shown that Arf has the capacity to arrest mouse embryonic fibroblasts (MEFs) that lack p21[115] or both p53 and Mdm2[116].

Loss of *Ink4a/Arf* is occurs in a subset of ccRCC patients

Ink4a/Arf is deleted in a wide variety of tumors such as bladder cancer, prostate cancer, glioblastoma, melanoma, non-small cell lung cancer, and a subset of ccRCC tumors. Studies of mice with deletions for Arf or Ink4a have revealed that they become more prone to spontaneous cancers than the wild type littermates. However, it would

appear that mice lacking both Ink4a and Arf are significantly more tumor prone than the single knockout mice[117,118]. Similarly, germline mutations in Ink4a/Arf in humans are associated with familial predisposition to melanoma and certain other cancers.

Most studies investigating 9p deletion in primary renal tumors found LOH of 9p21 locus to the most commonly reported copy number variation (CNV)[119,120]. In a study by El-Mokadem and colleagues, they found that 91% (32 out of 35) of the 9p deletions were due to LOH or monosomy. Only three tumors showed deletion of both copies. Researchers show that chromosome 9p (where *Ink4a/Arf* resides) deletion within a subset of ccRCC tumors is associated with decreased disease specific survival (DSS) and recurrence free survival (RFS)[121]. Additionally, previous research showed that aberrations leading to low expression of Ink4a and p14ARF are associated with aggressive ccRCC as well as a poorer prognosis[122,123].

CHAPTER 2: INVESTIGATING HIF-MYC INTERACTIONS WITHIN CLEAR CELL RENAL CELL CARCINOMA

Introduction

As previously described, HIF1α and HIF2α exhibit unique characteristics within RCC. Studies have shown that HIF2α promotes tumor growth in RCC xenograft models[124–126] whereas overexpression of stable HIF1α inhibits tumor growth[126,127]. In addition, cell cycle arrest can occur during hypoxia through HIF1α-dependent increase in cyclin-dependent kinase inhibitor (CKI) p21 and p27[128–130]. While p21 and p27 are not direct HIF1α target genes, their expression is due to HIF1α's ability to antagonize MYC activity by altering MYC's interaction with Sp1 (one of MYC's cofactors)—and subsequently relieving transcriptional repression at p21 and p27's promoters[131–133]. Conversely, work from Gordan and colleagues demonstrated that HIF2α has the ability to enhance MYC activity by stabilizing MYC's interaction with Max (another cofactor of MYC)—resulting in the activation of MYC target genes, Cyclin D2 and E2F1, involved in cell cycle progression[134]. Such work by Gordan and colleagues were conducted in cell lines that expressed either HIF1α (HCT116 cells, colon carcinoma cell line) or HIF2α (WT8 cells, 786-O RCC cells expressing pVHL). Research from the same group classified 57 independent sporadic ccRCC tumors based upon HIFα expression and *VHL* status. Such efforts revealed that tumors sorted into one of three categories: VHL wild type, both HIF1α and HIF2α expression, and HIF2α expression detected

exclusively. They found no tumors that only expressed HIF1α—suggesting that HIF2α may play a crucial role in the tumorigenesis of pVHL deficient ccRCC[135].

Such findings led us to question how MYC's transcriptional activity may be altered in ccRCC. It was important to utilize a system that reflected the observed HIFα status of ccRCC tumors (HIF1α and HIF2α versus HIF2α only) in order to appropriately discern MYC activity. In addition, only a few MYC target genes (p21, p27, Cyclin D2, and E2F1) were analyzed in experiments delineating MYC activity in the presence of either HIF1α or HIF2α. We set out to assess MYC transcriptional activity not only within the context ccRCC HIFα status, but also on a genome-wide scale.

Generating the appropriate ccRCC cell line

c-MYC transcriptional activity is differentially regulated in the presence of HIF1 or HIF2[134]. We set out to determine whether c-MYC's transcriptional activity is altered within the context of ccRCC. That is, in the presence of HIF2 only or HIF1 and HIF2 combined. In order to interrogate this question, we generated a RCC4 cell line with the following alterations: 1) doxycycline inducible expression of c-MYC as a means to control MYC expression and 2) has a loss of HIF1—thereby generating cells that express both HIF1 and HIF2 (referred to as H1H2) and HIF2 only (referred to as H2) (Figure 2.1a). RCC4s did not show any detectable levels of endogenous MYC at the protein level. The RCC4 cell line harbors the characteristic mutant VHL and is widely used as a representative ccRCC cell line[136]. This cell line also expresses both HIF1 and HIF2—making it a suitable cell line for our studies. Immunoblot analysis and normalized gene expression data confirmed the induction of MYC with doxycycline as well as knockdown of HIF1 (Figure 2.1b, Figure 2.3a,b).

Figure 2.1. Generation of H1H2 vs H2 cells with inducible MYC expression

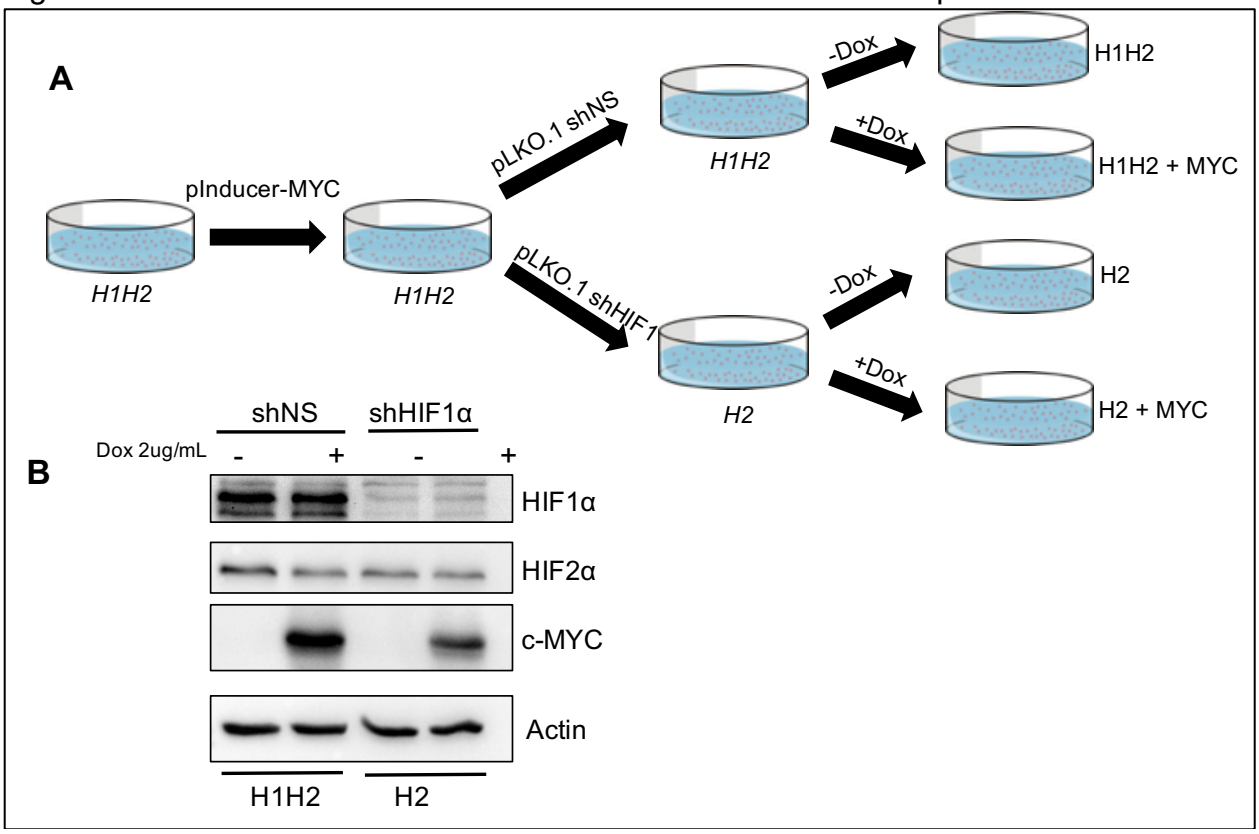

(A) Schematic of how RCC4 cell line was generated to yield the respective genetic groups for subsequent analysis. (B) Immunoblot from RCC4 cell lines shows c-MYC expression is doxycycline dependent. Additionally, knockdown of HIF1 was achieved using short hairpin against HIF1

H2 cells display evidence of enhanced cell cycle progression—but no significant global differences

In order to determine whether MYC induction resulted in the activation of genes associated in the canonical MYC pathway, we employed the use of a canonical c-MYC gene signature list, PID_MYC_PATHWAY. While there was a significant difference between cells with induced MYC expression (+MYC) and those without MYC induction (-MYC), there was no significant difference between H1H2 versus H2 cells with MYC induction. (Figure 2.2) This suggests that while the induction of MYC does yield significant differences of MYC related genes, this is not attributable to HIFα status.

Figure 2.2. Activation of MYC yields upregulation of canonical MYC pathway genes

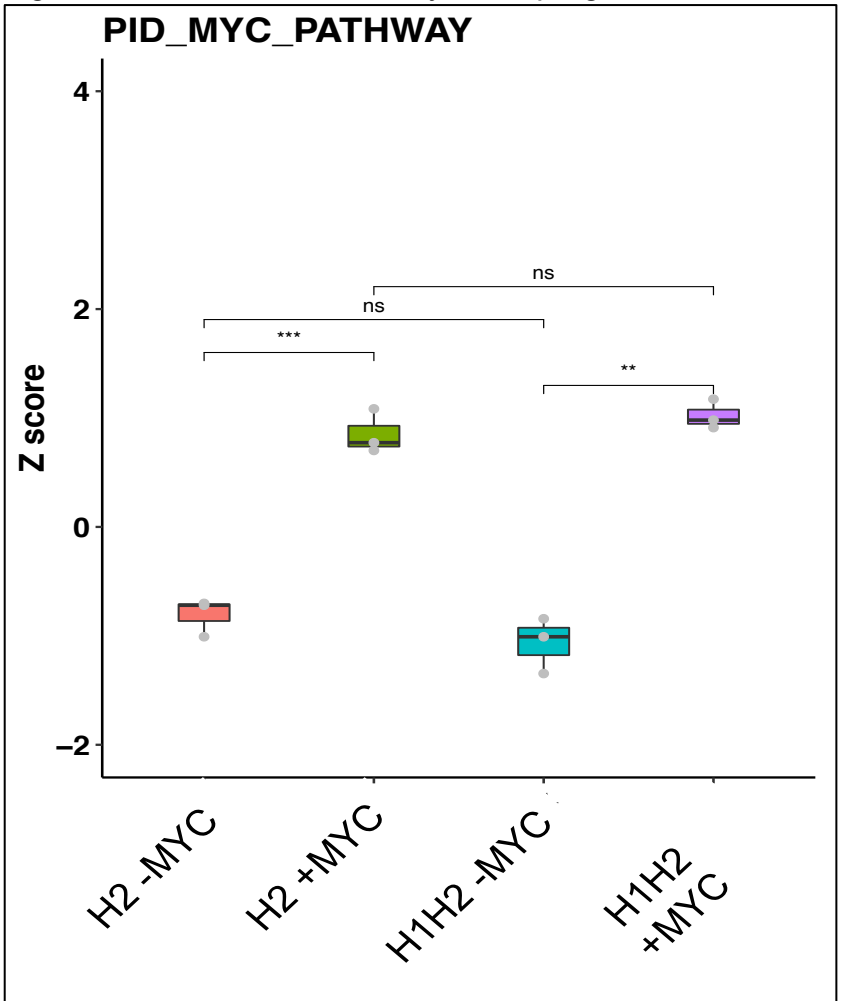

We hypothesized that H2 +MYC cells would show increased expression of genes involved in cell cycle progression compared to H1H2 +MYC cells. To investigate this, we analyzed the expression data of the MYC target genes assessed by Gordan et al[134,135]. The c-MYC activated target gene E2F1 was significantly higher in H2 expressing cells as compared to H1H2 cells. c-MYC repressed target gene, p21, was significantly reduced in H2 cells—confirming the observation that H2 cells promote cell cycle progression (Figure 2.3c,d)

Figure 2.3 H2 cells exhibit increased cell cycle progression

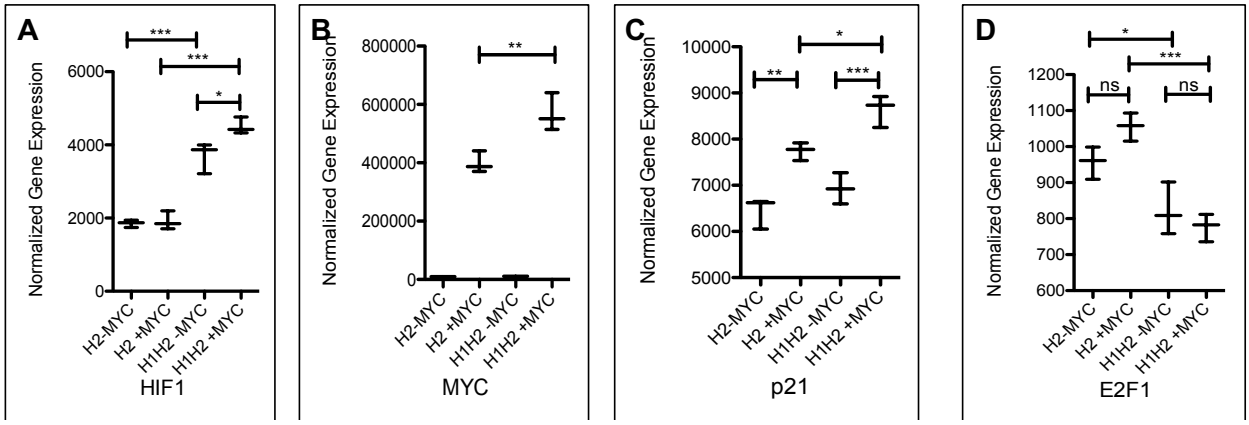

(A) Normalized gene expression profiles of HIF1, (B) c-MYC, (C) p21, and (D) E2F1. *P<0.05; **P<0.01, ***P<0.001. P values obtained from Tukey's test.

In addition, H2 cells exhibit elevated levels of genes involved in the G1/S cell cycle phase—further supporting evidence that HIF2α expressing cells are more proliferative than H1H2 cells (Figure 2.4).

Figure 2.4 HIF2 cells exhibit elevated levels of genes involved in G1/S phase

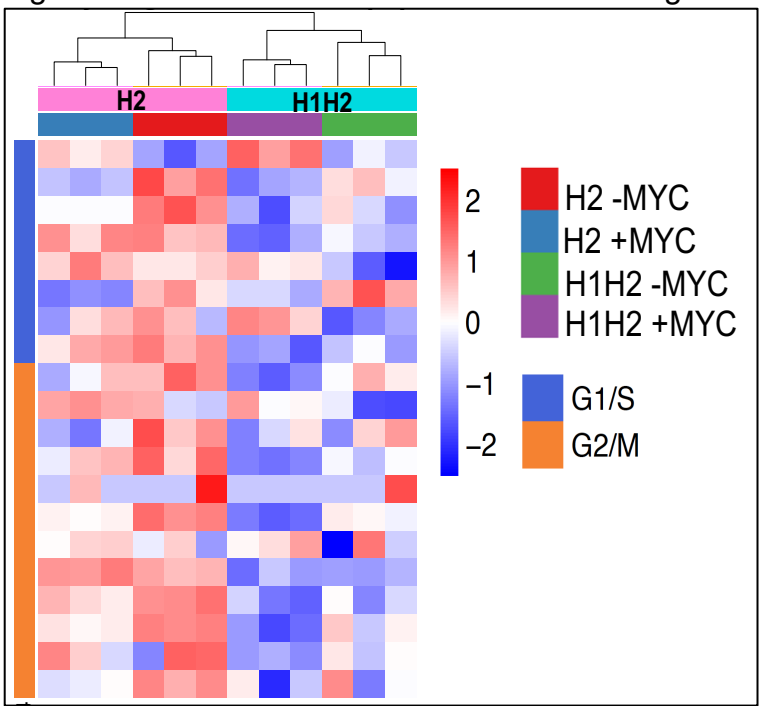

We next set out to determine whether there were significant MYC dependent gene expression differences between H1H2 and H2 cells on a genome-wide scale. As demonstrated in Figure 2.5, a scatterplot shows the fold change of genes induced or

repressed by MYC in H1H2 or H2 cells. MYC expression (+MYC/-MYC) between H1H2 and H2 cells revealed surprisingly very little genes that were significantly different between the two groups. This was evidenced by genes that were significantly altered in H2 (blue) or H1H2 (green) clustering below the 2-fold threshold. Additionally, the majority of genes that were significantly altered appeared in both groups (red)—suggesting that there is no difference in MYC's transcriptional activity between H1H2 and H2 cells.

Figure 2.5 MYC dependent gene expression is relatively unchanged genome-wide

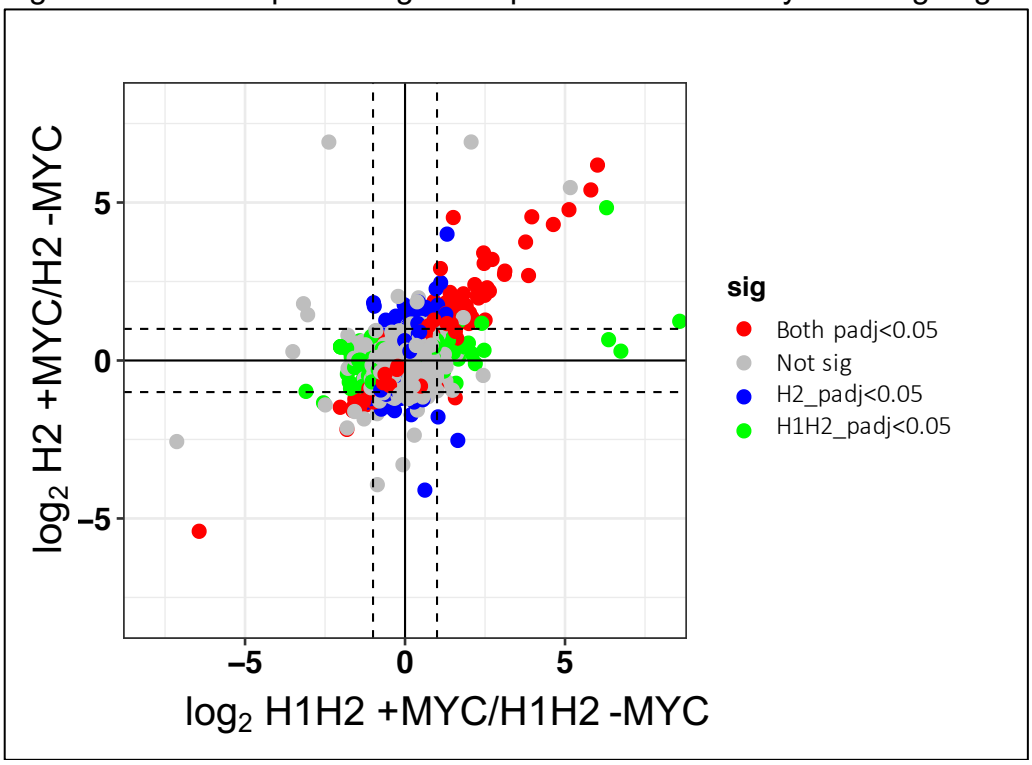

Discussion

Our group set out to determine whether MYC's transcriptional activity would be significantly altered in *VHL* deficient ccRCC cell lines expressing either HIF2α (H2) or HIF1α and HIF2α (H1H2). Generating cell lines of these two 'groups' of HIFα status

was important due to the fact that no ccRCC tumors only express HIF1α[135]. We also wanted to build upon the current knowledge that MYC activity is altered in the presence of HIF1α or HIF2α alone by interrogating this question on a genome-wide scale. I initially hypothesized that H2 cells would display a significantly distinct MYC transcriptional profile compared to H1H2 cells, based upon evidence that H2 ccRCC tumors showed evidence of elevated MYC activity compared to H1H2 ccRCC tumors. Our generated cell lines partially supported such evidence with the expression of a couple MYC target genes (p21 and E2F1). Gene expression data only showed cell cycle genes to be the only gene set significantly altered between H1H2 and H2 cells. Specifically, genes involved in the G1 to S phase transition.

This was, admittedly, a surprising and confounding result. H2 cells showed significantly elevated levels of E2F1 while H1H2 cells showed significantly elevated levels of p21 (Figure 2.3). This was promising seeing as that Gordan and colleagues also observed increased E2F1 in cells only expressing HIF2α[134] as well as HIF2α expressing ccRCC tumors[135]. However, subsequent gene set analysis revealed no global gene expression differences between H1H2 and H2 cells.

It is possible that our findings may be different given that we did not assess MYC activity in the context of HIF1α or HIF2α alone. Previous efforts were done in a colon carcinoma cell line (HCT116) and a pVHL restored RCC cell line (WT8). Furthermore, we did not account for endogenous levels of MYC due to the absence of any detectable expression at the protein level within RCC4. Additionally, we controlled for MYC expression by generating a doxycycline inducible system to drive exogenous expression of MYC. It is quite possible that our system represents an over-driven model of MYC

and such expression overwhelms any effect HIFs may be exerting within these cells—thereby masking any MYC dependent changes between H1H2 and H2 cells.

As such, follow up analysis would need to be performed to determine whether such observations are indeed true. This is discussed within the Final Discussion.

Methods

Immunoblotting conditions

RCC4 cells were cultured in 1XDMEM, 10% FBS, 1% PS containing 2 ug ml^{-1} doxycycline. In vitro doxycycline was dissolved in DMSO for approximately 18 hours. RCC4 cells were lysed in EBC lysis buffer complemented with Set I and Set II phosphatase inhibitors at 1X (Calbiochem), and protease inhibitors at 1X (Roche). Whole cell lysate concentration was determined with Bio-Rad Protein Assay Dye Reagent Concentrate (Bio-Rad). Proteins were resolved on SDS–PAGE gels and electro transferred onto PVDF membranes (Millipore). Primary antibodies: c-Myc (1:1,000; SC-42), HIF1 (Cell Signaling #3716), HIF2 (Cell Signaling #7096), and β-actin (HRP) (Cell Signaling #5125).

Cell culture conditions

RCC4 cells were maintained and cultured in 1XDMEM, 10% FBS, 1% PS. 2 ug ml^{-1} of doxycycline was added to media to induce MYC expression overnight. *In vitro* doxycycline was dissolved in DMSO.

RNA-seq analysis

RNA was isolated and purified for RNAseq analysis using the RNeasy Mini Kit (Qiagen) following manufacturer's protocol and eluted in water. A total of 200–1,000 ng of total RNA was used to prepare libraries with the TruSeq Stranded mRNA Sample

Prep Kit (Illumina). Around 75b paired-end reads were sequenced on a NextSeq 500 Desktop Sequencer using a high output flow cell kit (Illumina), yielding an average of approximately 50 M reads per sample. QC-passed reads were aligned to the human reference genome using STARv2.5.3a. Transcript abundance estimates for each sample were performed using SALMONv0.9.1. Raw SALMON read counts for all RNAseq samples were normalized and analyzed by DESeq2 (Bioconducter).

[*]CHAPTER 3: MYC ACTIVATION COOPERATES WITH VHL AND INK4A/ARF LOSS TO INDUCE CLEAR CELL RENAL CELL CARCINOMA[137]

Introduction

Renal cell carcinoma (RCC) is among the most common malignancies, with an estimated 65,000 new cases and 14,000 deaths annually in the United States[138]. RCC can be subclassified into distinct histologic subtypes including clear cell RCC (ccRCC), papillary RCC Types 1 and 2, and chromophobe RCC[139]. Inherited RCC can be caused by germline mutations in multiple genes that are linked to specific histologic subtypes. In particular, VHL, MET, FH and FLCN genes are linked to development of the clear cell, papillary Type 1, papillary Type 2 and chromophobe RCC subtypes, respectively[139–141]. Not surprisingly, these genes are often found to be mutated in sporadic cases of RCC as well[4,139–142].

The genetics of ccRCC have been studied in depth[141]. The von Hippel-Lindau tumour suppressor protein (pVHL) is broadly inactivated (~80%) in sporadic ccRCC by either mutation or promoter hypermethylation[140,143] and its tumour suppressor activity is dependent on its downregulation of the alpha subunits of the hypoxia-inducible factor (HIFα) family of transcription factors and in particular HIF2α[124,125,144,145]. In addition to

[*] This chapter previously appeared as an article in the journal Nature Communications. The original citation is as follows: Bailey, S. T., Smith, A. M., Kim, W. Y. MYC activation cooperates with Vhl and Ink4a/Arf loss to induce clear cell renal cell carcinoma. *Nature communications* 8, (2017).

mutations of VHL, whole exome sequencing studies have defined a number of other significantly mutated genes in ccRCC such as PBRM1, SETD2 and BAP1, many of which are related to histone modification or nucleosome remodeling[4,5,75,141]. ccRCC has a relatively low mutation burden relative to other solid tumours[64] but does have characteristic large deletions and gains of chromosomes 3p, 14q and 5q, respectively, as well as more focal gains and losses of 8q24 (harbouring MYC) and 9p21 (harbouring CDKN2A), respectively[4–6].

Focal amplification of 8q24 has been demonstrated in ~15–23% of ccRCC in three independent studies and in all studies the amplicon appears to harbour MYC[4–6] Gain of 8q, as assessed by classic cytogenetics, is associated with a high risk of lymph node and distant metastases and is an independent prognostic factor[113,146]. Despite this genetic evidence implicating MYC in ccRCC pathogenesis, the role of MYC in ccRCC is complex. Studies demonstrate that HIF2α can potentiate MYC transcriptional activity and that MYC gene signatures are able to define a subtype of ccRCC, while HIF1α has the potential to oppose MYC transcriptional activity[132,134,135].

Herein we describe the development of mouse models of papillary and clear cell RCC, by modelling the genetic events found in human kidney cancer. We uncover that MYC activation is sufficient to generate papillary RCC in mice. Moreover, MYC activation, along with Ink4a/Arf (Cdkn2a) inactivation cooperates with Vhl loss to form clear cell RCC that is occasionally metastatic. These GEM models represent the first tractable models of papillary and clear cell RCC that have a predictable latency with high penetrance. These models of papillary and clear cell RCC should therefore be significant contributions to the field of kidney cancer research.

Kidney specific MYC activation results in papillary RCC

Prior work has examined the role of MYC in the development of kidney cancer by overexpressing MYC under control of the gamma-glutamyl transferase promoter[147]. While the mice developed renal tumours, they appeared to be histologically and immunophenotypically most consistent with collecting duct carcinomas. We generated compound mutant mice engineered to express a doxycycline-inducible Myc transgene (Tet-O-MYC) targeted to the renal tubule cells under control of the Ksp promoter[8] (Ksp-rtTA; Tet-O-MYC mice; hereafter called 'MYC' mice) and control animals expressing only Tet-O-MYC. Mice were fed chow containing doxycycline starting at ~8 weeks of age to induce MYC expression and were followed for survival. MYC mice had a significantly shortened survival relative to controls (Figure 3.1a, P= 0.0162) and upon necropsy were found to harbour renal tumours but no evidence of macroscopic metastatic disease (Figure 3.1b).

Figure 3.1 Kidney specific MYC activation results in papillary renal cell carcinoma

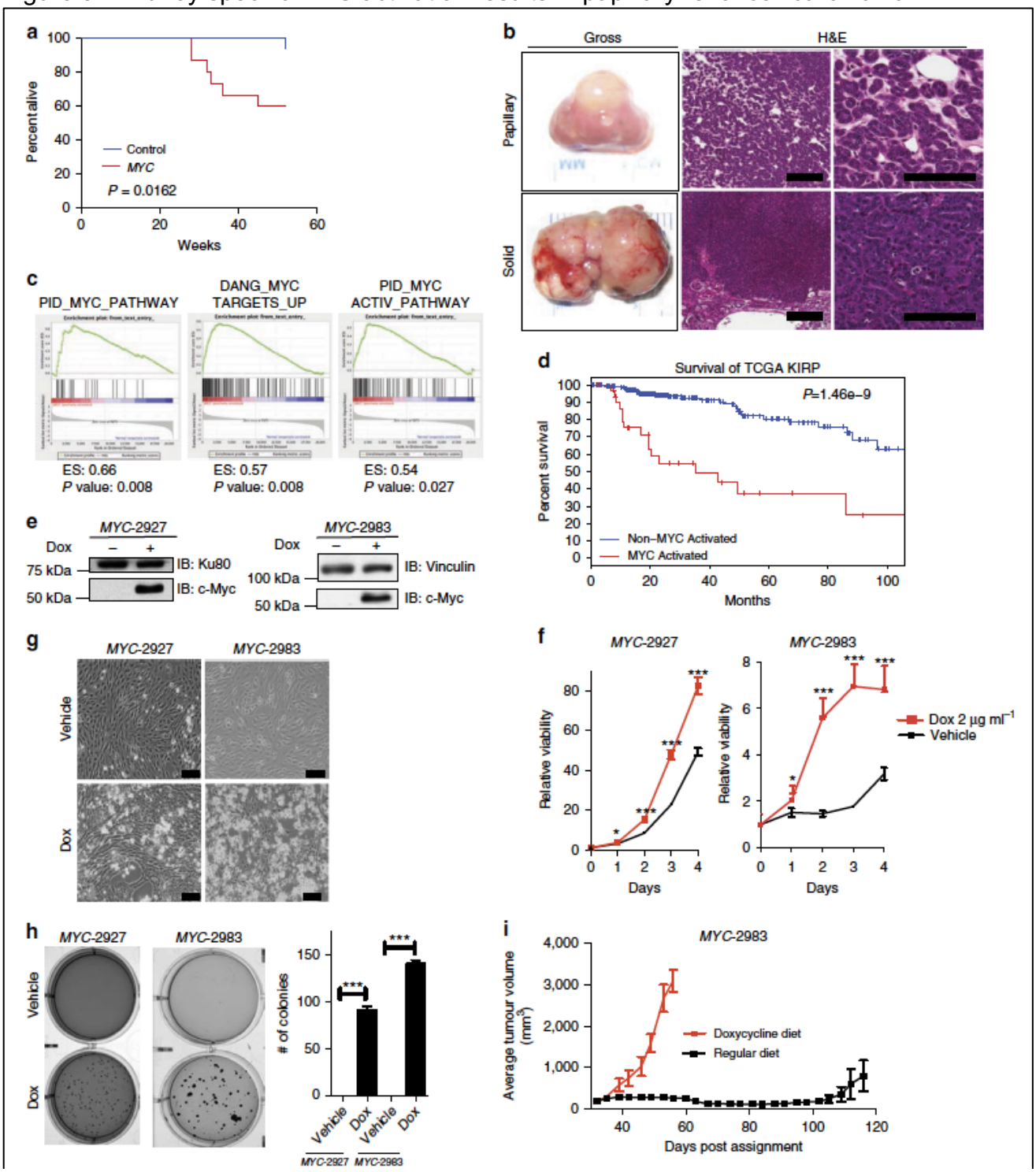

(a)Kaplan–Meier curve showing reduced survival rates in MYC mice (n ¼ 15) compared to controls (n ¼ 17) Log Rank P ¼ 0.0162. (b) Representative gross images and photomicrographs of H&E stained kidney sections from MYC mice (B32 weeks post Dox treatment) revealed both papillary (top panels) and solid kidney tumours (bottom panels) (scale bar, 100 mm). (c) GSEA enrichment plots showing papillary kidney tumours are

enriched for multiple gene sets representing MYC activation relative to normal kidney (GSE11151). (d) Kaplan–Meier curve of patients from the TCGA KIRP dataset demonstrating tumours with high MYC activity have reduced survival in patients with papillary renal cell carcinomas, Log Rank P ¼ 1.46e–9. (e) Immunoblot using whole cell lysates from MYC kidney tumor-derived cell lines (MYC-2927 and MYC-2983) shows expression of MYC is Dox dependent. (f) Cell viability assay show reduced proliferation from MYC-2927 and MYC-2983 cells upon Dox removal. Cells grown on Dox or vehicle were analyzed in replicates of n ¼ 8 each day. (g) Bright field image of MYC-2927 and MYC-2983 cells on day 3 after being cultured with or without Dox. (scale bar, 100 mm). (h) Soft agar assays show anchorage independent growth of MYC-2927 and MYC-2983 cells is significantly reduced upon removal of Dox. Images are representative of each condition performed in triplicate. (i) Results from xenograft studies showing tumours formed from MYC-2983 cells remain dormant upon removal of Dox in vivo (n ¼ 5 per group). (f,g) *Po0.05, ***Po0.0001.(f,h,i) Data are presented as mean ± s.e.m. (f,h) P values obtained from student t-test.

Histologic examination showed that the majority of the tumours found in the kidneys of MYC mice had either a papillary or a more solid and infiltrative appearance. Smaller tumours (<3 mm) were predominantly papillary (Figure 3.1b ‘papillary’), while larger tumours (>3 mm) were either papillary or consisted of more solid appearing tumours characterized by tightly packed papillary structures lacking distinct fibrovascular cores (Figure 3.1b ‘solid’). These larger, solid tumours were characterized by hyperchromatic cells with a high nuclear to cytoplasmic ratio. In addition, the cells contained nuclei with large nucleoli, significant pleomorphism and were high grade (Supplementary Figure 3.1A). Notably, intra-tumoral foamy macrophages and psammoma bodies (features that are commonly seen in human papillary renal cell carcinoma) were lacking in the MYC tumours

Supplementary Figure 3.1 MYC activation in the kidney results in histological abnormalities

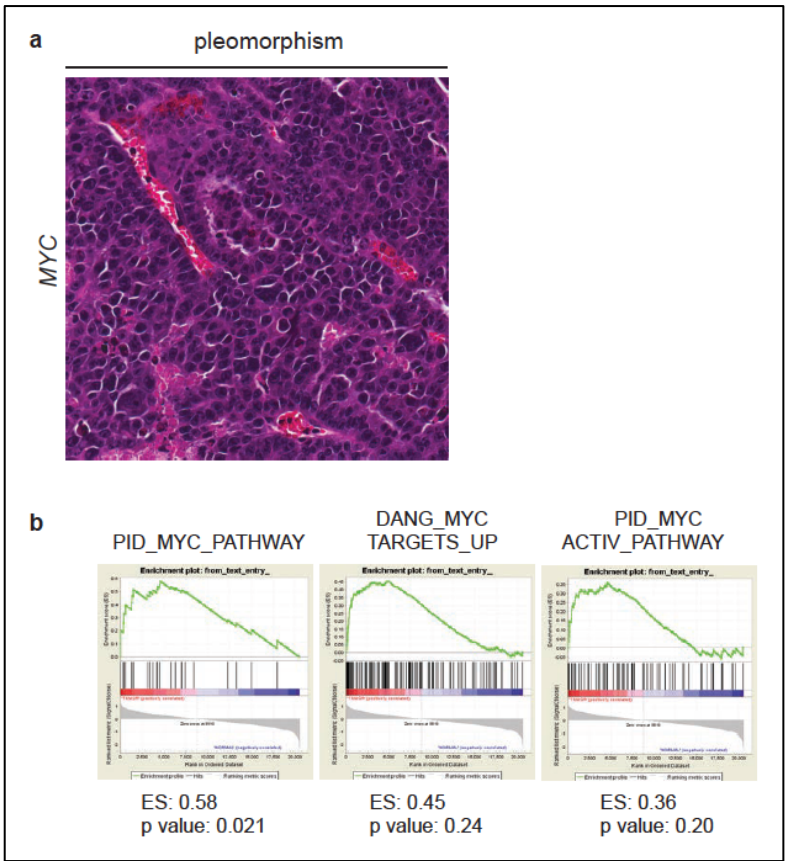

(a) H&E staining of a representative kidney section from a MYC mouse reveals pleomorphism. (b) GSEA enrichment plots showing papillary tumors from TCGA KIRP are enriched for gene sets representing MYC activation relative to normal kidney.

Papillary RCC with MYC activation has a worse prognosis

Prior work has shown that a subset of pRCC, primarily Type 2 pRCC, is enriched for gene signatures of MYC activation and that tumours with MYC activation have a worse overall survival.[8] We confirmed and extended these findings using multiple gene expression datasets, which revealed that pRCC tumours were enriched for MYC activation gene signatures when compared to normal kidney (Figure 3.1c and Supplementary Figure 3.1b)[148]. Finally, to determine the impact of MYC activation on prognosis, we classified TCGA KIRP tumours as MYC activated (n=23, defined as

tumours with a Z score of the PID_MYC_ACTIV_PATHWAY greater than 1.0 s.d. above the mean) or not MYC activated (n=153). Consistent with previous work, patients with MYC activated pRCC tumours had a significantly worse overall survival (Figure 3.1d, p=1.46e-9)[8].

Cell lines from *MYC* mice are dependent upon MYC expression

To better characterize the phenotype of the kidney tumours from MYC mice we generated two cell lines from separate *MYC* tumours (*MYC*-2927 and *MYC*-2983). After verifying the Dox responsiveness of the *Tet-O-Myc* transgene in these MYC cells (Figure 3.1e), we examined the effect of MYC expression on cell proliferation *in vitro*. MYC cells grown in the presence of Dox (activated MYC) had increased proliferation at 4 days (Figure 3.1f), as well as a visible increase in cell number (Figure 3.1g). In addition, while MYC cells with Dox were unable to form colonies in soft agar, MYC cells grown in Dox formed colonies robustly in an anchorage independent manner (Figure 3.1h). Finally, we assessed the ability of MYC-2983 cells to form tumours in vivo and their in vivo growth dependence on MYC expression. To this end, $5x10^6$ MYC-2983 cells were injected subcutaneously and monitored for growth in mice fed Dox chow. Once tumours reached ~300mm^3, mice were either continued on or withdrawn from Dox (Figure 3.1i). As expected, tumours of mice that remained on Dox continued to have rapid growth, while tumours in mice withdrawn from Dox remained dormant. Therefore, *MYC*-induced papillary RCCs are dependent upon *MYC* expression for *in vitro* and *in vivo* growth.

Vhl loss with MYC activation promotes clear cell changes

Focal amplification of 8q24 is found in 15% of ccRCC in the TCGA KIRC data set[4]. To ensure that MYC was located in the minimal common region (MCR) of amplification, we used GISTIC 2.0 analysis to identify a broad statistically significant (q value<0.25) region of amplification on chr8. This MCR contains MYC. A plot of mean gene-level DNA copy number measurement by genomic position (Supplementary Data 1 and Supplementary Figure 3.2a) shows that mean MYC copy number is larger than the 70% of the mean gene-level DNA copy values. Therefore, while these data suggest that MYC is an important target of amplification in this region there are still ~100 genes with mean copy number values that are higher. Similarly, focal loss of 9p21 was found in 32% of ccRCC in the TCGA KIRC data set[4]. GISTIC 2.0 analysis demonstrated the presence of only three genes in the minimal common region of copy number loss, *CDKN2A*, *CDKN2B* and *C9orf53* (Supplementary Figure 3.2b). These results suggest that both *MYC* and *CDKN2A* may be involved in the development or progression of ccRCC.

Supplementary Figure 3.2 GISTIC copy number by gene

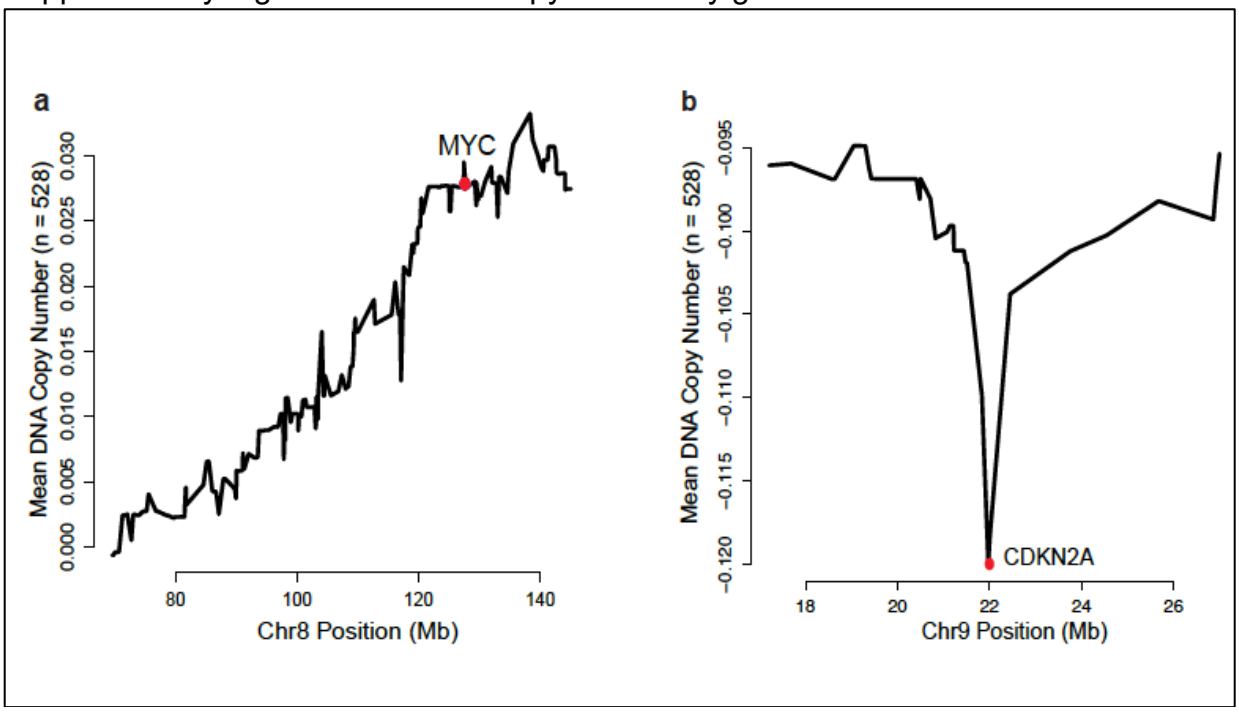

(a) GISTIC2 analysis on TCGA KIRC cohort of patients showing average DNA copy number measurements within region of amplification in chr8 for MYC and (b) region of deletion of chr9 for CDKN2A.

To model the interplay of genomic events observed in human RCC, we next examined the phenotypes of kidney specific Vhl inactivation in combination with MYC overexpression or combined MYC overexpression and Ink/Arf deletion. Specifically, MYC mice were crossed to conditional Vhl knock-out mice (*Vhl*$^{F/F}$)[54], *Cdkn2a* (*Ink4a/Arf*$^{-/-}$) germline knock-out mice[149], as well as mice expressing tamoxifen-inducible Cre recombinase under control of the Ksp cadherin promoter (*KspCre*^{ERT2}) to generate cohorts of *KspCre*^{ERT2}; *Vhl*$^{F/F}$ control mice (conditional inactivation of *Vhl*, hereafter called *V*), *KspCre*^{ERT2}*; Vhl*$^{F/F}$; *Ksp-rtTA; Tet-O-Myc* (conditional inactivation of Vhl and Dox-inducible MYC overexpression, hereafter called VM), and *KspCre*^{ERT2}; *Vhl*$^{F/F}$*; Ink/Arf*$^{-/-}$*; Ksp-rtTA; Tet-O-Myc* (conditional inactivation of Vhl, germline Ink/Arf$^{-/-}$, and

Dox inducible *MYC* overexpression, hereafter called *VIM*) (see Supplementary Table 3.1).

Supplementary Table 3.1 Summary of RCC GEM models

Abbreviation	Genotype	Functional Effect
MYC	*Ksp-rtTA; Tet-O-MYC*	• Dox inducible *MYC* expression
V	*KspCreERT2; $Vhl^{F/F}$*	• conditional inactivation of *Vhl*
VM	*KspCreERT2; $Vhl^{F/F}$; Ksp-rtTA; Tet-O-Myc*	• conditional inactivation of *Vhl* • Dox inducible *MYC* expression
VIM	*KspCreERT2; $Vhl^{F/F}$; Ink/$Arf^{-/-}$; Ksp-rtTA; Tet-O-Myc*	• conditional inactivation of *Vhl* • germline *Ink/$Arf^{-/-}$* • Dox inducible *MYC* expression

Cohorts of *V*, *VM*, and *VIM* mice were followed for survival (Figure 3.2a). *VM* mice had a significantly worse survival than *V* mice (P=0.007) and *VIM* mice had a significantly worse survival than both *V* and *VM* mice (both P<0.001, Figure 3.2a). Histologic examination showed that the kidneys of *V* mice were essentially normal (Figure 3.2b). In contrast, kidneys from *VM* and *VIM* mice had a high incidence of tumour formation (67% and 100% respectively, Table 3.1).

Figure 3.2 MYC activation combined with Vhl and Ink4a/Arf loss results in histopathological changes in the kidney resembling human clear cell renal carcinomas

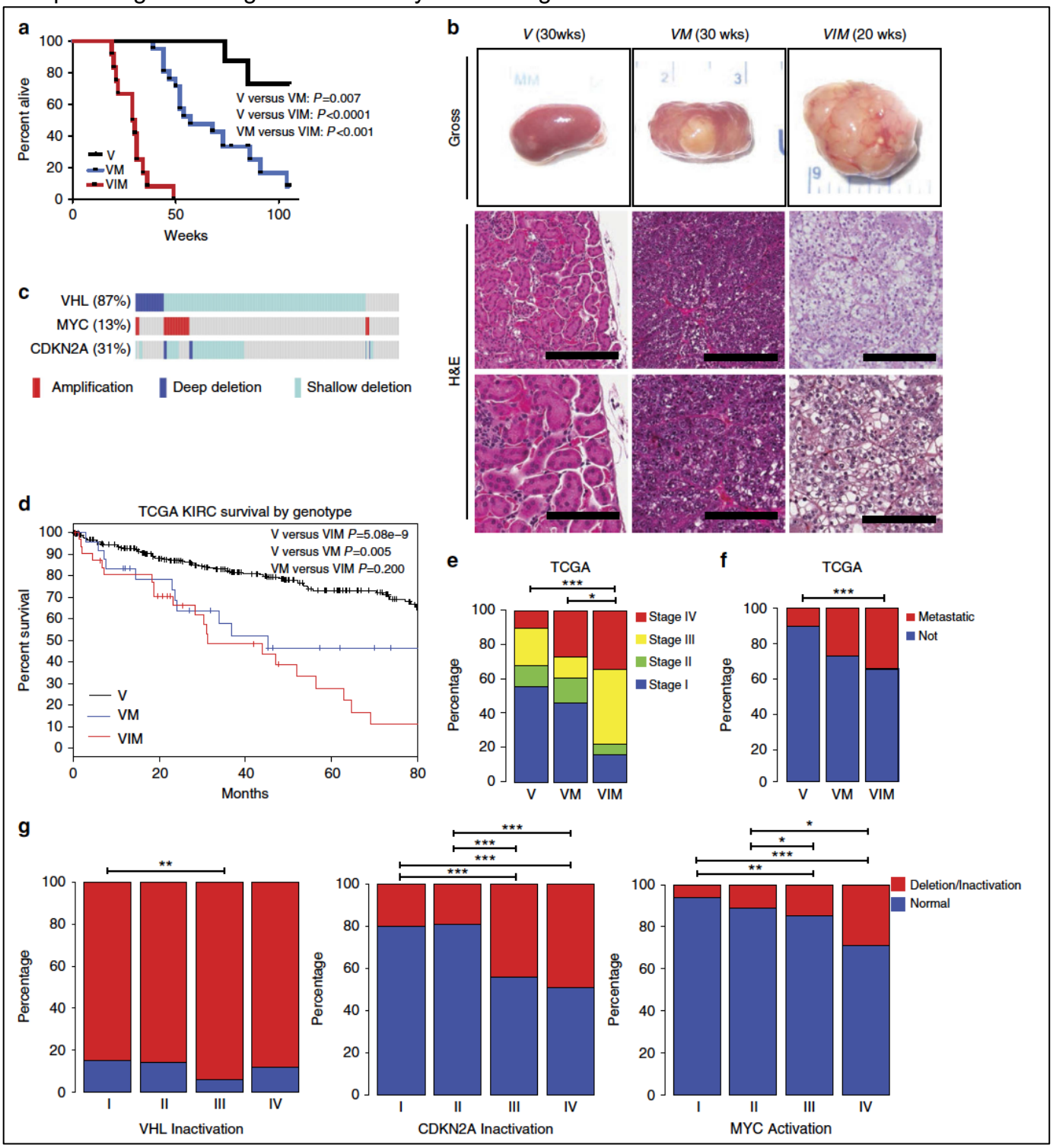

(a) Kaplan-Meier survival curve comparing survival rates between V (n.8), *VM* (n.21) and *VIM* (n.12) mice. Log rank V versus *VM* P.0.007, *V* versus *VIM* P<0.0001, *VM* versus *VIM* P<0.001. (b) Representative gross and H&E images of kidney sections from V (33 weeks), *VM* (30 weeks) and *VIM* (19 weeks) mice at the indicated times post Dox

treatment. (scale bars, 200 and 100 mm). (c) cBioPortal OncoPrint plot showing the distribution of *MYC*, *VHL* and *CDKN2A* copy number alterations in the TCGA KIRC data set. (d) Kaplan–Meier survival curve comparing human kidney renal clear cell carcinomas with *V*, *VM* and *VIM* alterations. Log rank *V* versus *VIM* P.5.08e-9, *V* versus *VM* P.0.005, *VM* versus *VIM* P.0.200. (e) Bar graph showing the correlation of *V*, *VM* and *VIM* tumours from the TCGA KIRC dataset with stage and (f) metastasis. (g) Bar graphs showing percentage of TCGA KIRC tumours with alterations in VHL, CDKN2A, and MYC by TNM Stage. (e–g) *P<0.05; **P<0.01, ***P<0.001. P values obtained from Chi-square test.

Table 3.1 Comparison of VM and VIM mice

	VM	**VIM**
Median survival (weeks after Tam/Dox)	57	29.5
Cysts present	9/9 (100%)	6/6 (100%)
Kidney tumour present	6/9 (67%)	6/6 (100%)
Large kidney tumour (>3mm)	2/9 (22%)	4/6 (67%)
Low grade	3/9 (33%)	1/6 (17%)
High grade	3/9 (33%)	5/6 (83%)
Necrosis present	1/9 (11%)	4/6 (67%)
Bona fide clear cell histology	0/9 (0%)	5/6 (83%)
Liver metastases	0/9 (0%)	2/6 (33%)

Kidney tumours of *VM* mice had either a tubulo-papillary or solid appearance with intervening vessels. The tumour cells were hyperchromatic compared to the normal renal tubular epithelium. Occasional clear cell features were identified (Figure 3.2b; Supplementary Figure 3.3). Small tumours were generally well demarcated, while larger tumours showed a multilobulated growth pattern with frequent necrosis, haemorrhage and dystrophic calcifications (Supplementary Figure 3.4A).

Supplementary Figure 3.3 Representative H&E images of VM and VIM mouse tumors

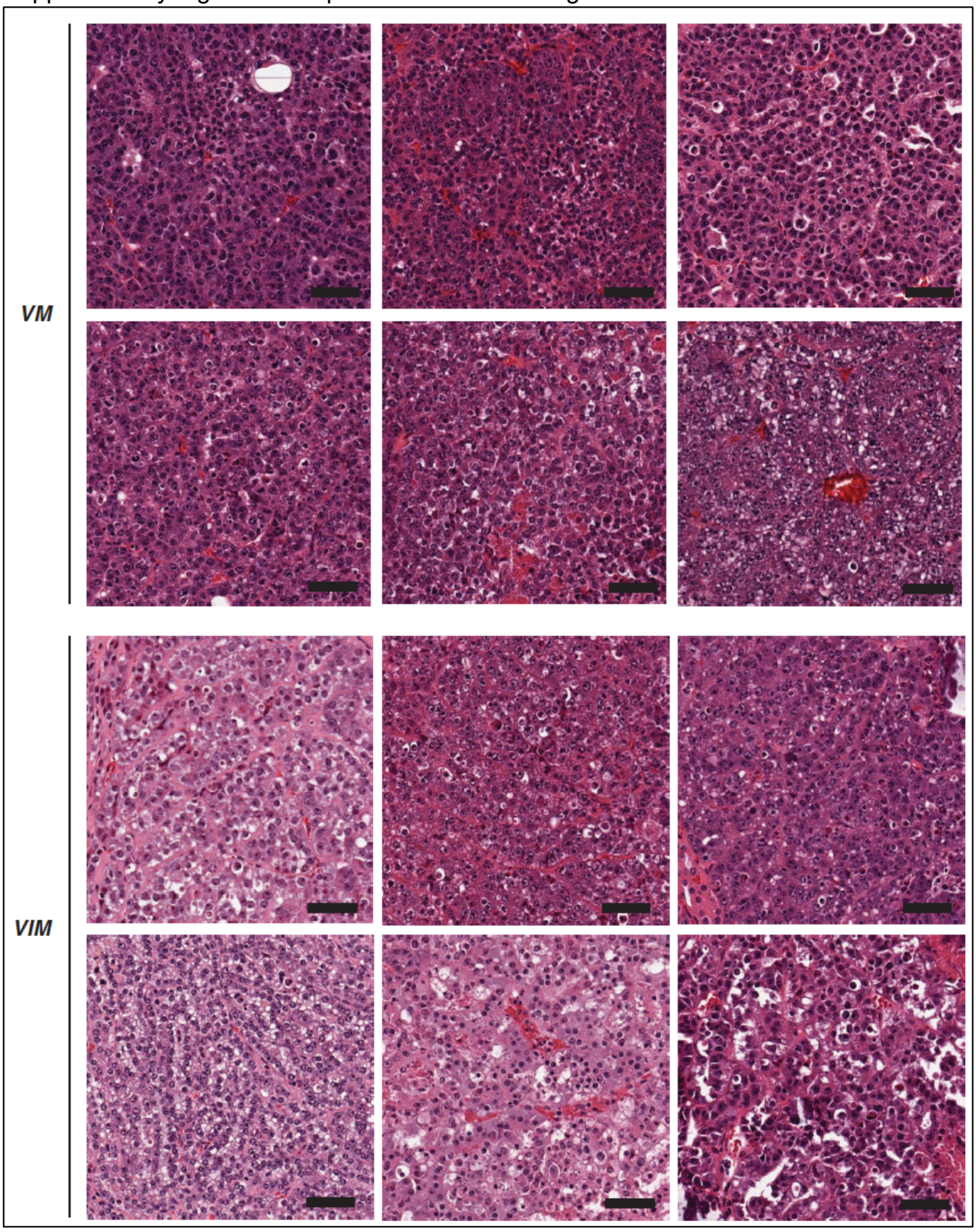

Scale bar = 50um

Supplementary Figure 3.4 VM and VIM mice have histological abnormalities in their kidneys

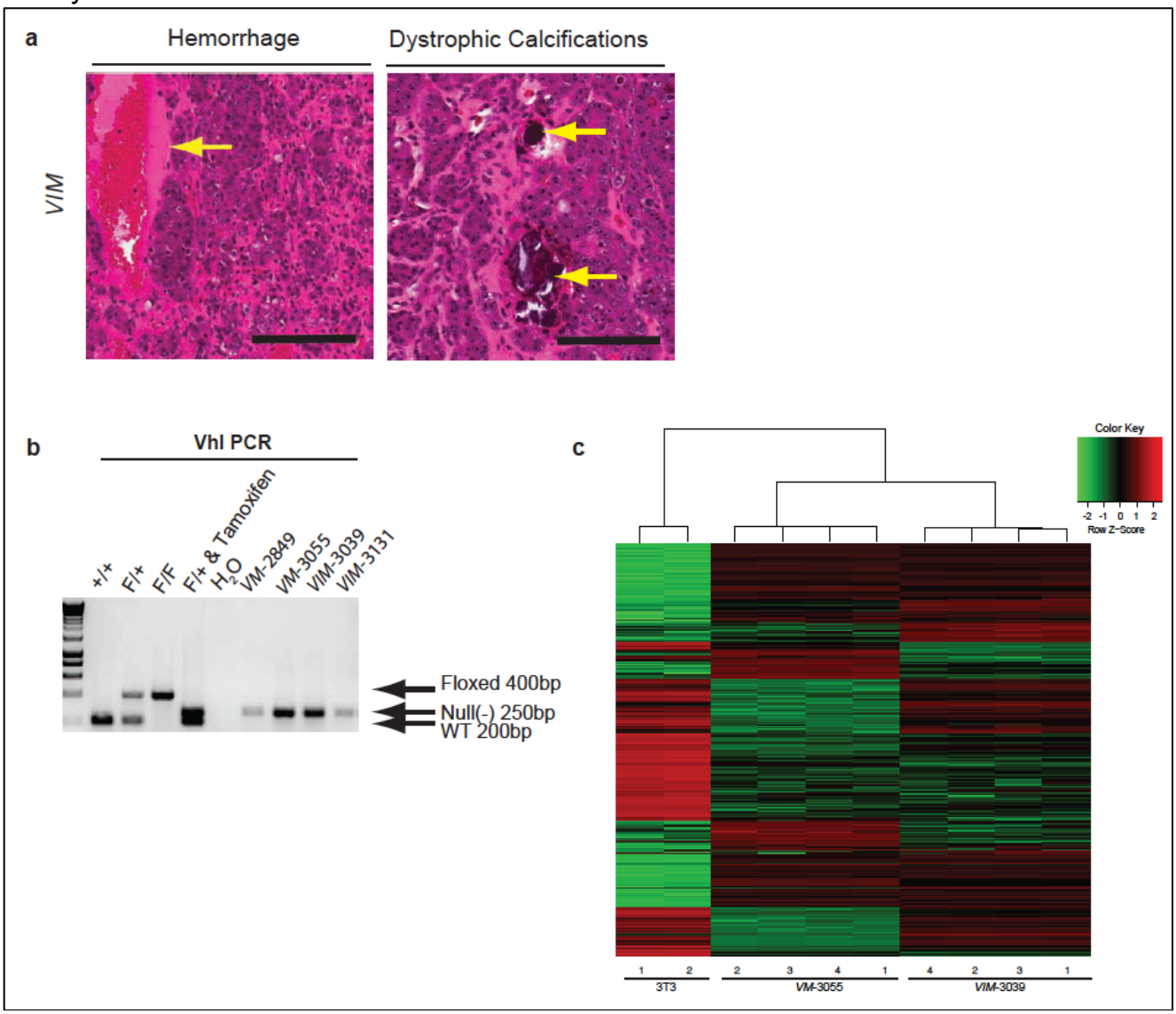

(a) H&E staining of a representative kidney section from a *VM* tumor. Arrows point to areas of hemorrhage and dystrophic calcifications. (b) PCR verification of Vhl deletion in the *VM* and *VIM* cell lines. (c) Heat map showing distinct expression patterns between 3T3 fibroblasts and *VM*-3055 and *VIM*-3039 cell lines

While tumours similar to those seen in the *VM* mice were observed in *VIM* mice, the kidneys of *VIM* mice also harboured tumours with a solid or tightly packed tubulo-papillary appearance. The cells were small to intermediate in size with increased nuclear to cytoplasmic ratio with nuclei that were round to oval with prominent single nucleoli (Supplementary Figure 3.3). Clear cell changes within the larger tumours were

also present with areas within some tumours showing what appeared to be histology strikingly similar to human ccRCC (Figure 3.2b). These areas were typified by nests of tumour cells with an increased amount of clear to granular cytoplasm, separated by thin vascular channels. Therefore, while *Vhl* loss combined with *MYC* activation is sufficient to induce modest clear cell changes, *Vhl* loss combined with *MYC* activation and *Ink/Arf* deletion induces bona fide clear cell RCC (Table 3.1).

ccRCC with *VM* and *VIM* alterations have worse prognosis

We next examined whether human ccRCC tumours with similar genomic characteristics (*VHL* inactivation; *VHL* inactivation and *MYC* activation; and *VHL* inactivation, *CDKN2a* loss and *MYC* activation) have similar outcomes as those seen in our mouse models. Of TCGA KIRC tumours (n=525), 87, 13, and 31% had *VHL* inactivation, *MYC* activation and *CDKN2A* deletion, respectively (Figure 3.2c). We further classified these patients as *V* (n=286, 54%), *VM* (n=26, 5%) and *VIM* (n=32, 6.1%) and noted that *VM* and *VIM* patients had a significantly decreased survival relative to V patients (P=0.005 and P=5.086x10^{-9}), respectively (Figure 3.2d), but that *VM* and *VIM* patients had a similar overall survival. In keeping with the notion that *VIM* tumours are more clinically aggressive, we also noted significant enrichment of higher stage and presence of metastases in patients with *VIM* tumours relative to patients with V tumours (Figure 3.2e,f). When limiting our analysis to stage IV tumours, we did not see significant survival differences by genotype (*V*, *VM*, and *VIM*) (Supplementary Figure 3.5). Because of the very limited patient numbers (*V*=28, *VM*=7, and *VIM*=11), we examined whether *VIM* genotype was prognostic when controlled for both TNM stage and Furhman grade. Cox proportional hazards (Cox PH) modelling using the V

genotype as the reference demonstrated that the *VIM* genotype was prognostic was still prognostic (Cox PH=1.79, P=0.034). Therefore, *VIM* tumours appear to have worse clinical characteristics and outcome in human ccRCC patients even when controlling for stage and grade.

Supplementary Figure 3.5 No difference in survival among stage IV patients

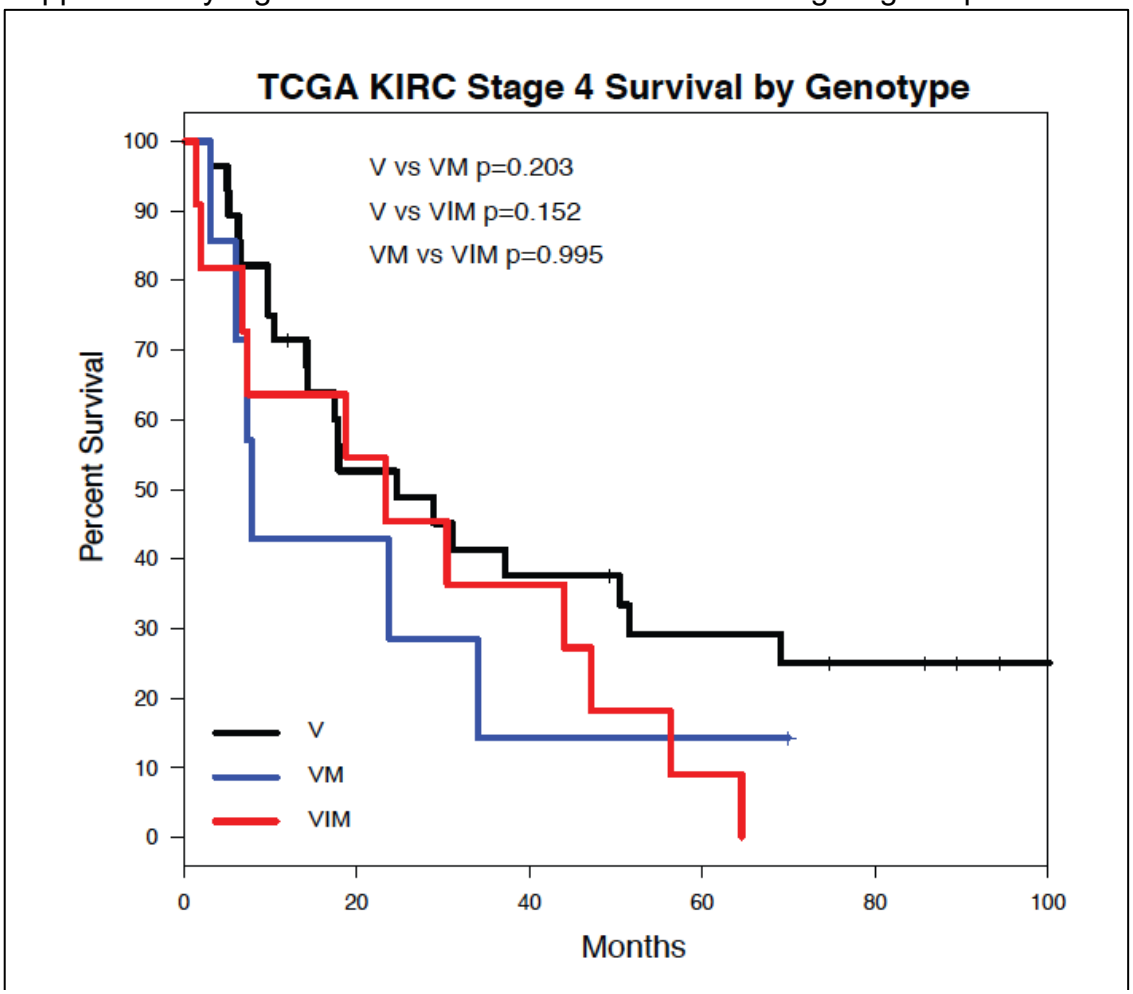

Kaplan-Meier survival curve of TCGA KIRC stage IV KIRC patients with V, VM, or VIM genotype. V (n=28), VM (n=7), VIM (n=11). Log rank V vs VM p=0.203, V vs VIM p=0.152, VM vs VIM p=0.995

VM and *VIM* cell lines are dependent upon MYC expression

We generated cell lines from VM and VIM tumours to assess their dependency on MYC expression. We first confirmed the Dox inducibility of the MYC transgene in these *VM* (2849 and 3055) and *VIM* (3039 and 3131) cells (Figure 3.3a), as well as the

fact that they had undergone Cre mediated recombination of the Vhl locus (Supplementary Figure 3.4b). Furthermore, we set out to confirm that VM-3055 and *VIM*-3039 cell lines are epithelial in nature. We performed RNAseq and co-clustered mouse 3T3 fibroblasts with *VM*-3055 and VIM-3039 cell lines using the top 10% of the most differentially expressed genes (Supplementary Figure 3.4c). 3T3 fibroblasts show a distinctly different expression pattern from both *VM*-3055 and VIM-3039 cell lines showing that our *VM* and *VIM* cell lines are not fibroblastic in nature. After confirming that the *VM* and *VIM* cells were derived from renal epithelium, we assessed their growth in in vitro assays. Similar to MYC cells, the proliferation and anchorage independent growth of VM and VIM cells were dependent on MYC expression (Figure 3.3b–d).

To understand the MYC dependent changes on the transcriptomes of *VM*-3055 and *VIM*-3039 cells, we performed RNAseq on these cells grown in tissue culture in the presence or absence of Dox. There were a large number of genes that were differentially regulated (increased or decreased greater than two-fold; t-test FDR<0.05) by MYC activation (Dox) in both *VM*-3055 (799 up and 2491 down) and *VIM*-3039 (1017 up and 2159 down) cells (Figure 3.3e). While there was overlap among genes that were upregulated by Dox in both *VM*-3055 (634 of 799) and VIM-3039 cells (634 of 1017) (Figure 3.3e), nearly a third of Dox inducible genes in *VIM*-3039 cells (378 of 1017) were not upregulated in *VM*-3055 cells. A similar percentage of genes repressed by MYC activation (Dox) in *VIM*-3039 cells were not repressed in *VM*-3055 cells either, suggesting that MYC may regulate both an overlapping and a unique spectrum of genes in *VM*-3055 and *VIM*-3039 cells.

Figure 3.3 VM and VIM tumours are dependent on MYC expression

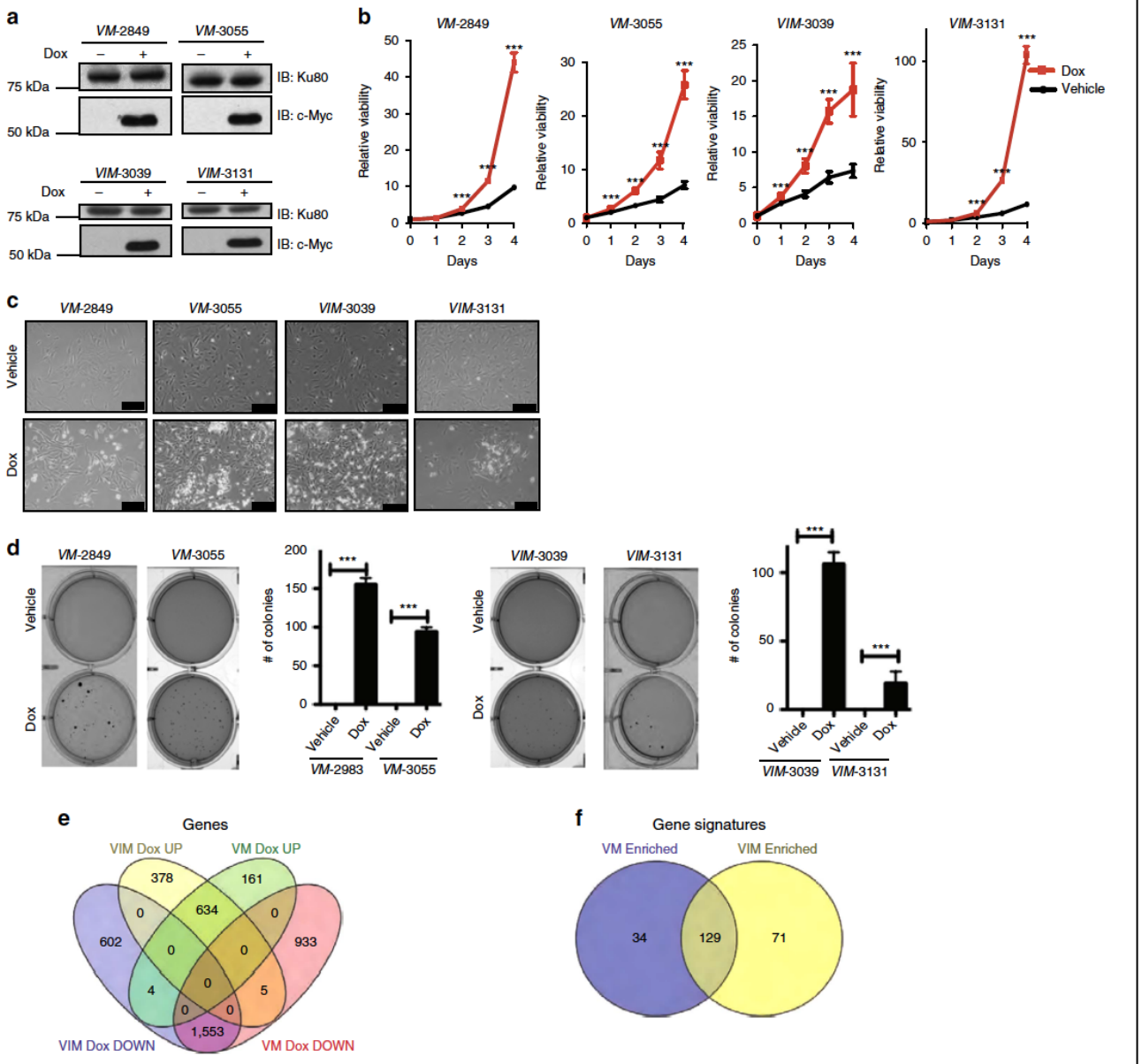

(a) Immunoblot of whole cell lysates from *VM* (*VM*-2849 and *VM*-3055) and *VIM* (*VIM*-3039 and *VIM*-3131) tumour-derived cell lines shows expression of MYC is Dox dependent. (b) Proliferation of *VM* and *VIM* cells is significantly reduced with removal of Dox. Cells grown on Dox or vehicle were analysed in replicates of n=8 each day. (c) Bright field image of *VM* and *VIM* cells three days after Dox removal show a decrease in cell number (scale bar, 100 mM). (d) Soft agar assays show anchorage independent growth of *VM* and *VIM* cells is reduced upon Dox removal. Images are representative of each condition performed in triplicate. (e) Venn diagram showing overlapping and distinct sets of genes altered upon Dox removal in *VM*-3055 and *VIM*-3039 cells. (f) Venn diagram showing Dox dependent gene expression in *VM*-3055 and *VIM*-3039

activates distinct gene sets. (b,d) ***P<0.0001. P values obtained from student t-test. Data are presented as mean ±s.e.m

We next performed gene set analysis. Gene sets that were enriched in *VM*-3055 cells cultured in Dox relative to those cultured without Dox included a number of gene signatures characteristic of MYC activation including those related to cell cycle progression and ribosome biogenesis (Supplementary Data 3.2). A parallel analysis in *VIM*-3039 cells also demonstrated high enrichment in proliferation and ribosome biogenesis gene signatures (Supplementary Data 3.3), but also included gene signatures related to DNA methylation, as well as RNA binding. Indeed, the top gene signatures significantly enriched in *VM*-3055 and *VIM*-3039 cells (an area under the curve (AUC) greater than 0.25) were relatively non-overlapping (Figure 3.3f). While these findings are in keeping with the notion that MYC activation induces many unique gene expression changes specific to *VM*-3055 and *VIM*-3039 cells given the analysis is on a single-cell line, they will need to be validated in future studies.

GEM tumours correlate with human RCC

Given that MYC tumours resemble human papillary tumours histologically, while *VM* and *VIM* tumours resemble ccRCC, we wanted to determine if the similarities would also be apparent at the gene expression level. Pearson correlations on whole transcriptome centroids between MYC (n¼4), *VM* (n¼4) and *VIM* (n¼4) mouse tumours and the TCGA KIRC and KIRP data revealed that *VM* and *VIM* tumours correlated most highly with TCGA KIRC tumours, while MYC tumours correlated more highly with TCGA KIRP tumours (Figure 3.4a). Further verifying the importance of MYC activity in pRCC Type 2, a cross species analysis of mouse MYC tumours with the TCGA KIRP data set

demonstrated co-clustering of MYC tumours with human papillary Type 2 tumours (Figure 3.4b). Moreover, transcriptome wide Pearson correlations revealed that MYC tumours more closely resemble TCGA KIRP tumours verified to be Type 2 pRCC (Figure 3.4c). Collectively, these analyses support the clinical relevance of the MYC, *VM* and *VIM* mouse models with human papillary and clear cell renal cancers.

Figure 3.4 Renal carcinoma mouse models reflect the transcriptomic landscape of human renal carcinoma

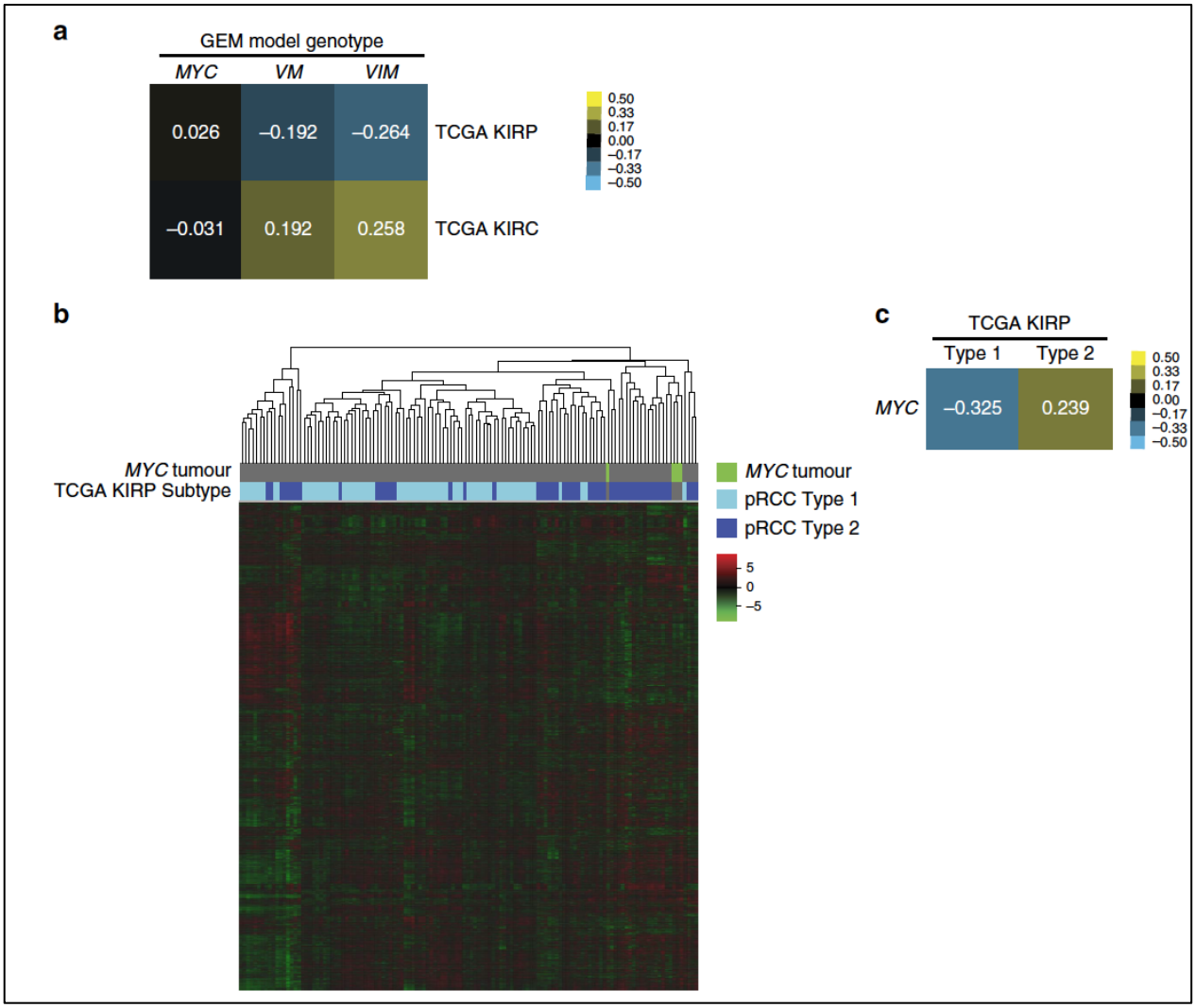

(a) Pearson correlation of whole-transcriptome centroids of M/VM/VIM mouse models and papillary renal cell carcinoma (KIRP)/clear cell renal cell carcinoma (KIRC) TCGA tumor samples. (b) Heatmap clustering of M mouse model samples with TCGA KIRP samples identified by subtype. (c) Pearson correlation of whole-transcriptome centroids of the M mouse model with KIRP TCGA Type 1/Type 2 samples.

Ink4a/Arf loss in *VM* mice promotes metastases

During necropsies of *VIM* mice, we noted that a number of mice had what appeared to be macroscopic metastases to the liver at a low frequency (Figure 3.5a,b, and Table 3.1). Histologically, the liver metastases were either tubulo-solid or clear cell with cytologic features consistent with the primary renal tumour. Metastases were identified in the subcapsular area and within the parenchyma. Notably, vascular spaces were involved by tumour in some of the liver specimens (Figure 3.5a). We did not see any macroscopic metastases to other organs such as the lung.

Given the metastatic phenotype seen in the *VIM* mice but not in the *VM* mice, we examined a panel of genes that characterize epithelial to mesenchymal transition (EMT) (Cdh1 (E-cadherin), Cdh2 (N-cadherin), Vim (vimentin)), as well as a panel of transcription factors well known to regulate EMT (Snai1, Snai2, Zeb1, Zeb2, Twist1) in the RNAseq data from our cell lines. *VIM*-3039 cells demonstrated gene expression changes that were consistent with a state of EMT with decreased expression of E-cadherin (Cdh1) and increased expression of N-cadherin (Cdh2) and Vimentin (Vim) as well as upregulated expression of Snai1, Snai2, Twist1, Zeb1 and Zeb2 (Figure 3.5c). In addition, we noted that a number of the most differentially expressed genes (Supplementary Data 3.4) are implicated in invasion and metastasis through remodeling of the extracellular matrix such as the lysyl oxidase family members Lox, Loxl1, Loxl2 and hyaluronan synthase 2 (Has2)[150–154]. (Figure 3.5d). Given these differences in gene expression, we examined the invasiveness of our *VM*-3055 and *VIM*-3039 cell lines in vitro in matrigel invasion assays. As predicted, *VIM*-3039 cells had significantly increased matrigel invasion (Figure 3.5e). Therefore, Ink4a/Arf inactivation appears to

facilitate EMT, invasion and metastases and the metastatic phenotype seen in vivo is recapitulated in vitro.

Figure 3.5 Combinatorial loss of Vhl and Ink4a/Arf with MYC activation promotes metastasis and activation of EMT genes

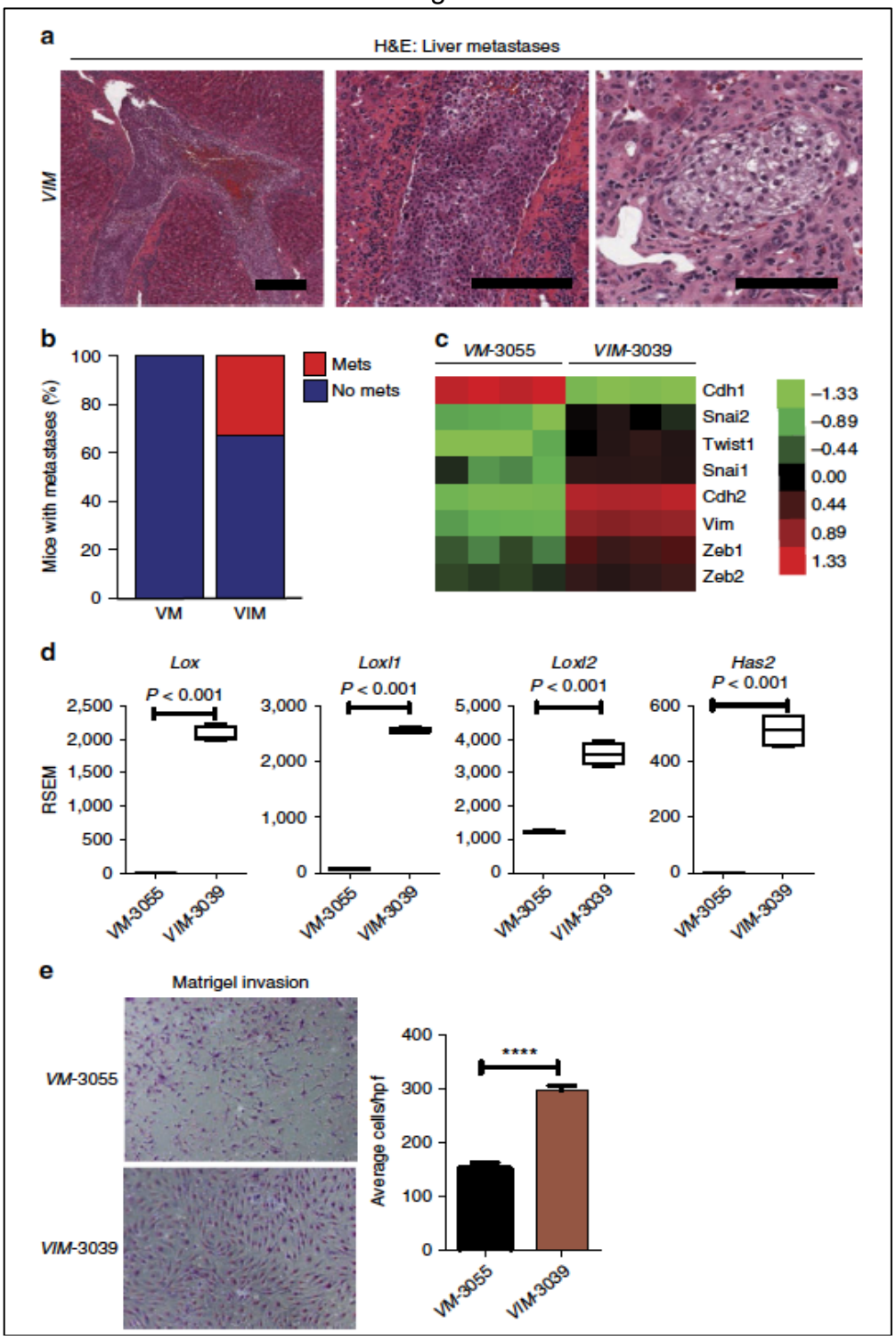

(a) A representative H&E stained liver sections from a *VIM* mouse shows metastasis to the liver parenchyma as well as intravascular mets. Higher power magnification reveals features resembling renal clear cell carcinomas within the metastatic lesions. (Scale bar, 100 mm). (b) Bar graph showing percentage of mice with metastases. (c) Heat map showing the expression patterns of EMT associated genes in *VM*-3055 and *VIM*-3039 cells. (d) Higher expression of genes involved in invasion and metastasis is observed in *VIM*-3039 cells compared to *VM*-3055 cells. (e) Matrigel invasion assays show increased invasion from *VIM*-3039 cells compared to *VM*-3055 cells. ****P<0.0001. (d,e) P values obtained from student t-test. Data are presented as mean ±s.e.m.

VHL restoration has no effect on *VIM* cells

Previous work in human ccRCC cell lines has shown that VHL does not affect in vitro proliferation or anchorage independent growth[12]. To assess whether this was true in our *VIM* cell lines, we established isogenic *VIM* cells expressing eGFP or HA-VHL (Figure 3.6a). As predicted, there were no VHL dependent differences in in vitro growth (Figure 3.6b) or ability to form colonies in soft agar (Figure 3.6c). These results are in keeping with those seen in human ccRCC cell lines. At this time, we have not been able to reliably generate allograft tumours from our *VM* or *VIM* cell lines and therefore cannot interrogate whether VHL plays a tumour suppressor role in vivo, as previously shown with human RCC cell lines[12]. Therefore, whether our GEM models are overdriven remains a possibility.

Figure 3.6 Restoration of VHL does not significantly reverse tumorigenic capacity of VIM cells

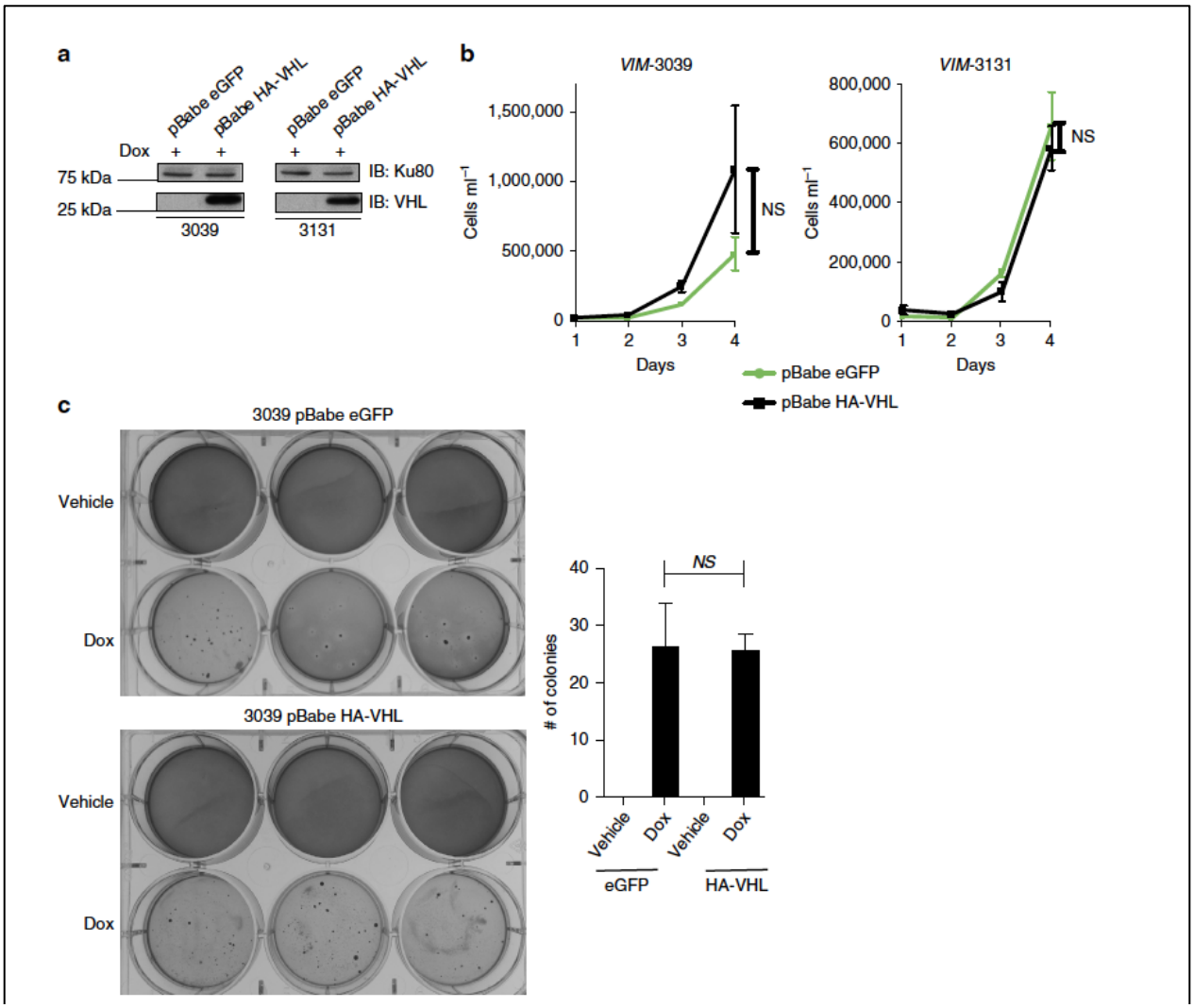

(a) Immunoblot of whole cell lysates from VIM cells infected with pBabe eGFP and pBabe HA-VHL. (b) Cell growth assay shows no significant reduction in cell number in VIM cells when VHL is expressed. Cells grown on Dox or vehicle were analyzed in triplicate each day. (c) Soft agar assays show VIM-3039 cells form colonies in an anchorage independent manner despite the presence of VHL. (b,c) P values obtained from student t-test. Data are presented as mean ±s.e.m.

Discussion

The development of GEM models of cancer has had significant impact on functional genomics as well as preclinical development of novel therapies. Indeed, robust GEMMs of non-small cell lung cancer[155] and pancreatic ductal adenocarcinoma[156] have led to an explosion of research into the biology underlying these diseases and facilitated the study of diverse fields such as biomarker discovery and investigations into the cell of origin of various cancers. Our own studies highlight the role of MYC in renal tumorigenesis and demonstrate that MYC activation is sufficient to generate papillary RCC and that when combined with Vhl and Ink4a/Arf inactivation results in bona fide clear cell renal cell carcinoma.

Development of robust GEM models of kidney cancer has been a long-sought after and elusive goal despite substantial efforts in this area. Multiple groups have now demonstrated that Vhl inactivation either in the germline or by conditional inactivation in the kidney results in only a mild increase in rate of renal cyst formation[53–55,57,60]. While the addition of secondary genetic events such as Pten or Kif3a loss appear to accelerate the cystic phenotype induced by Vhl inactivation, they do not result in frank neoplasia[59,70]. Combined inactivation of Vhl with Trp53 does appear to induce renal tumours, which have clear cell changes but not bona fide clear cell RCC histology[66]. A recent report demonstrated that combined inactivation of Vhl with Bap1 results in renal tumours with clear cell histology[78]. However, while inactivation of other tumour suppressor genes such as Flcn, Tsc1 or Fh results in renal carcinomas[157–161], they are rarely of the clear cell histologic subtype and they exhibit long latency, impacting their

utility for routine investigation. Therefore, there remains a need for RCC models that are highly penetrant, relatively rapid and that display robust papillary or clear cell histology.

Schroff and colleagues recently reported the phenotype of kidney specific overexpression of c-MYC in mice[147]. They found robust development of renal tumours that were dependent on upregulated glutaminolysis. Histological and immunohistochemical analysis demonstrated that these tumours were most consistent with collecting duct carcinomas. Collecting duct carcinomas are thought to arise from the collecting ducts, which are embryologically derived from the metanephros and distinct from the nephron. In support of this, the immunophenotype, as well as response to therapy are closely associated with urothelial carcinomas (bladder cancer)[162] and as such, they are treated with bladder cancer specific chemotherapy regimens such as MVAC (methotrexate, vinblastine, adriamycin, and cisplatin). Our studies also examined the phenotype of kidney specific overexpression of c-MYC. However, in contrast to Schroff and colleagues our MYC mice developed renal tumours with histology highly reminiscent of human papillary RCC. We hypothesize that these distinctions may be due to the relative differences in expression patterns of the promoters used to overexpress MYC (Schroff et al. use g-glutamyl transpeptidase while our studies use Ksp-cadherin), as well as any potential differences in the timing of MYC activation.

Our mouse models of pRCC and ccRCC faithfully recapitulate the genomics of human RCC although the incidence of ccRCC tumours that have coincident *VHL* and *CDKN2A* inactivation, along with MYC activation is only ~6%. The genomics of papillary and clear cell RCC implicate MYC as a potential oncogenic driver event[4–6] and our studies firmly place MYC as playing an active role in their pathogenesis. VHL

inactivation results in the stabilization of the alpha subunits of the hypoxia-inducible factor alpha (HIF) family of transcription factors of which HIF2α is thought to be a key oncogenic driver of ccRCC tumorigenesis, while emerging evidence suggests that HIF1α may be a tumour suppressor gene[124,127,140,144,145,163]. Past work examining the potential interaction between HIFα subunits and MYC suggest that while HIF1α disrupts MYC transcriptional activity, particularly of those genes involved in cell cycle progression, HIF2α actually facilitates MYC/MAX interactions[134,135,164]. It will be interesting to determine whether these HIF and MYC interactions occur in vivo in our *VM* and *VIM* mouse models and whether these oncogenic dependencies can be used as therapeutic vulnerabilities.

The *Ink4a/Arf* locus is best known as a cell autonomous barrier to cellular transformation through its negative regulation of cell cycle progression and its ability to promote cellular senescence[165]. Our studies demonstrate that *Ink4a/Arf* inactivation promotes liver metastases in an autochthonous ccRCC GEM model and that *Ink4a/Arf* loss is associated with gene expression patterns of EMT. Several past studies support that *Ink4a/Arf* may regulate EMT and metastasis. For example, in the mid 1990s, Allan Balmain and colleagues noted that p16 loss was a critical event in the regulation of an invasive spindle cell phenotype of mouse skin carcinomas, which today would likely be termed EMT[166]. In addition, a recent genome wide CRISPR screen in a cell line xenograft model identified *CDKN2A* as strongly associated with increased metastases[167]. At this time, we hypothesize that *Ink4a/Arf* loss does not directly regulate EMT or metastases but that its loss is permissive for the emergence of clones that allow metastatic behaviour. Nonetheless, our studies bolster the notion that *Ink4a/Arf* loss is a

metastatic driver event and demonstrate this association in autochthonous ccRCC GEM models.

In summary, we present GEM models of papillary and clear cell RCC that are faithful to the genomic events and recapitulate the histology seen in their respective human correlates. These pRCC and ccRCC GEM models should be a valuable contribution to the field of kidney cancer research and given their immune competent state should be invaluable in the development of immune based therapy.

Methods

GEM models

Conditional Vhl knock-out mice ($Vhl^{F/F}$)[54], germline Cdkn2a (Ink4a/Arf) knockout mice ($Ink4a/Arf^{-/-}$) [54] KspCad-CreERT2[144], KspCad-rtTA[168] and Tet-O-Myc mice have all been previously described. Tet-O-Myc was a generous gift from Dr Dean Felsher. Protocols for all animal experiments described were approved by the UNC-CH Institutional Animal Care and Use Committee.

Reagents for *in vivo* studies

Conditional activation of cre recombinase was induced by oral administration of tamoxifen (Sigma T5648). Per ml of *in vivo* oral delivery, tamoxifen was formulated as: 100 mg of tamoxifen dissolved in 100 ml 100% EtOH, followed by the addition of 1 ml of sunflower oil to achieve 100 mg ml^{-1}. The solution was sonicated in a water bath sonicator located at 4°C for 10 second pulses. The solution was then placed in a water bath at 50°C for 1 minute until clear. Sonication and water bath steps were repeated until no particulates were noticeable. Animals were given 50 ul (5mg per day) for three consecutive days by oral gavage. Tamoxifen oral solution was aliquoted and stored at

20°C and brought to administrable solution by 50°C water bath for no longer than 5min. The Tet-ON conditional system was activated with doxycycline chow (Research Diets, Inc. C11300–2000 with 2,000 p.p.m. doxycycline) 7 days post oral tamoxifen administration.

Primary tumour cell line generation and culture conditions

Primary renal GEMM tumours were excised and washed in a solution of Pen-Strep, PBS solution (1:1). In sterile conditions, primary tumours were cut into 2 x 2 mm fragments and dissociated in a gentleMACS C-Tube (Miltenyi Biotec) using the gentleMACs Dissociator (program: m_imp Tumor_02) in 5ml of 1XDMEM, 10% FBS, 1% PenStrep. 100 ul of collagenase D/dispase II (Roche: 40 mg ml^{-1}) was added to the tumour fragments and continuously inverted for 30 min at 37°C. Fragments were then subjected to a second round of dissociation using the gentleMACS Dissociator (program: m_imp Tumor_03). A total of 5 ml of protein extraction buffer (PEB: buffer 0.5% FBS, 2mM EDTA in PBS) was added to the dissociated fragments and resuspended by pipetting. The cell suspension was transferred to a 50 ml conical tube through a 40 mm nylon mesh sterile cell strainer (Fisher). An additional 20 ml of PEB buffer was added to the cell suspension and then centrifuged at 300g for 5 minutes. Supernatant was removed and cell pellet was resuspended in 6ml of 'conditioned media'[169] containing 2 ug ml^{-1} doxycycline (Sigma) and placed in a 6 cm sterile cell culture plate. On reaching confluency, cells were split and cultured in 1XDMEM, 10% FBS, 1% PS containing 2 ug ml^{-1} doxycycline. In vitro doxycycline was dissolved in DMSO.

Xenograft

Primary renal GEMM tumour cell lines were implanted subcutaneously into SCID mice flanks at 5 x 10^6 cells in 200 ml of PBS containing 2 ug ml^{-1} doxycycline. To maintain expression of c-MYC, SCID mice harboring xenografts were placed on doxycycline chow and withdrawn from doxycycline at the indicated times.

Immunoblotting conditions

Cells were lysed in RIPA buffer complemented with Set I and Set II phosphatase inhibitors at 1X (Calbiochem), and protease inhibitors at 1X (Roche). Whole cell lysate concentration was determined with Bio-Rad Protein Assay Dye Reagent Concentrate (Bio-Rad). Proteins were resolved on SDS–PAGE gels and electrotransferred to nitrocellulose membranes, 0.2 mm (Bio-Rad). For detection of c-MYC protein, proteins were electrotransferred onto PVDF membranes (Millipore). Primary antibodies, c-Myc (1:1,000; SC-42), VHL (1:500; SC-5575), Ku80 (1:1,000; Cell Signaling #2,180), Vinculin-HRP (1:1,000; Cell Signaling #18799); SC: Santa Cruz Inc. (Supplementary Figure 3.6).

Cell viability assay

Cell viability in the context of the various culture conditions was measured by CellTiter-Glo Luminescent Cell Viability Assay (Promega) per manufacture's protocol. Cells were counted and in a 96 well opaque side/clear bottom cell culture plates (Corning). Luminescence measurements were captured using a Biotek Synergy 2 plate reader. Statistical significance was measured by student t-test.

Soft agar assay

Anchorage independent growth was assayed following a standard soft agar assay protocol (bottom layer, 0.6% Difco Noble Agar (BD Biosciences) and top layer 0.4% Noble agar (Difco)). 200 ml of control media or media containing 2 ug ml^{-1} doxycycline was added to hydrate top agar every 72 hours. A total of 5,000 cells were plated in each well of a tissue culture treated 6 well plate (Corning). Colonies were stained with crystal violet solution for 4 h and destained with H_2O. Pictures were taken using a digital camera (Cannon). Treatment conditions were performed in triplicate. Statistical significance was measured by t-test.

Mouse RNAseq

An equal number of cells (2 x 10^5 cells per dish) were plated with or without Dox and collected for RNA 24 h later. RNA was isolated and purified for RNAseq analysis using the RNeasy Mini Kit (Qiagen) following manufacturer's protocol and eluted in water. A total of 200–1,000 ng of total RNA was used to prepare libraries with the TruSeq Stranded mRNA Sample Prep Kit (Illumina). Around 75b paired-end reads were sequenced on a NextSeq 500 Desktop Sequencer using a high output flow cell kit (Illumina), yielding an average of over 28 M reads per sample. QC-passed reads were aligned to the mouse reference genome (mm9) using MapSplice[170]. The alignment profile was determined by Picard Tools v1.64 (http://broadinstitute.github.io/picard/). Aligned reads were sorted and indexed using SAMtools and translated to transcriptome coordinates then filtered for indels, large inserts and zero mapping quality using UBU v1.0 (https://github.com/mozack/ubu). Transcript abundance estimates for each sample were performed using RSEM, an expectation-maximization algorithm (Li and Dewey,

2011) using the UCSC knownGene transcript and gene definitions[171]. Raw RSEM read counts for all RNAseq samples were normalized to the overall upper quartile[172].

Gene set analysis was performed between two groups of samples by first ranking all genes by t-statistic between groups. A K–S test was performed to determine if the genes in each gene set from MSigDB were uniformly distributed among the ranked list. K–S test P values were corrected via B–H procedure with an overall FDR of 5%. ROC curves were then generated for each gene set using the ranked list of t-statistics, and the AUC for the top 10% of ranked genes was used to rank gene sets among those passing the K–S test.

Analysis of human renal gene expression data from TCGA

GSE11151 data set was downloaded on Jan 27, 2015 from Gene Expression Omnibus (GEO) website. RNA Expression dataset was log2-transformed/median centered across pRCC and normal tissue samples. RNA expression dataset was analyzed with the Gene Set Enrichment Analysis (GSEA) desktop platform.

TCGA KIRP dataset was downloaded on Feb 1, 2015 from Broad TCGA website. RNA Expression dataset was log2-transformed/median centered. RNA expression data set was analyzed with the GSEA desktop platform.

TCGA KIRC data sets were downloaded on Feb 15, 2015 from Broad TCGA website. RNA Expression dataset was log2-transformed/median centered. RNA expression dataset was analyzed with the cBioPortal Oncoprint function and on R platforms.

Analysis of human copy number data from TCGA

Gene-level segmented DNA copy values for the TCGA KIRC cohort (**n.**528) were downloaded from the Broad Institute GDAC (https://gdac.broadinstitute.org/). The GISTIC2 analysis (Mermel, 2012) identified a statistically significant ($q<0.25$) region of amplification in chr8 (69506698-146364022). Mean gene-level DNA copy number measurements were computed and plotted by genomic position.

Correlation analyses

The TCGA clear cell renal cell carcinoma (KIRC) and papillary renal cell carcinoma (KIRP) RNASeq expression datasets were downloaded through the Broad Institute pipeline (Broad Institute TCGA Genome Data Analysis Center (2016): Aggregate Analysis Features. Broad Institute of MIT and Harvard). Human homologues were identified for mouse genes from the Jackson Laboratory Mouse Genome Informatics database (http://www.informatics.jax.org/homology.shtml). When combining datasets, batch effects were adjusted for using the SVA (surrogate variable analysis) R package version 3.12.0. Centroids were derived by taking the median expression of each gene across samples in a designated sample cohort. Centroid similarity metrics were derived by calculating the Pearson correlation between centroids. Heatmap clustering was done using centered average linkage clustering on all expressed genes in the data set.

Matrigel invasion assay

RCC GEMM cell lines were plated in serum-free medium for 24 hours. A total of 50,000 cells were seeded into an 8-mm matrigel chamber (BD Biosciences) and placed in wells containing medium containing 10% FBS. Cells were allowed to invade for 24

hours. Cells that had invaded through the matrigel were then stained with the Siemens Staining Kit according to manufacturer's directions. Matrigel wells were then placed on a glass slide and analyzed and photographed using an Olympus IX51 microscope. Representative pictures were taken of each matrigel well quadrant, and the number of cells that had invaded into the matrigel was determined by counting the number of stained nuclei using ImageJ.

Data availability

Raw RNA sequencing data are available from NCBI GEO under accession no. GSE97654.

CHAPTER 4: FINAL DISCUSSION

Chapter 2 discussion and future directions

As described above, we did not find any differentially expressed MYC dependent genes on a global scale to between H1H2 and H2 expressing cells. While this was surprising, work from Lin and colleagues demonstrated similar findings. They showed that MYC accumulates in the promoter regions of active genes across the genome and causes transcriptional amplification—but does *not* lead to newly activated or repressed *MYC* target genes. This was observed when authors compared two small cell lung carcinoma (SCLC) cell lines with either high (H2171 SCLC) or low (H128 SCLC) MYC expression. Gene expression analysis revealed that while H2171 cells had approximately 150-fold more c-MYC protein compared to H128, the set of transcribed genes were similar in low and high MYC expressing cell lines—indicating that elevated c-MYC levels do not significantly increase the number of expressed genes.

While it is possible our results support this model, further analysis would need to be done to confirm this theory. It would be interesting to perform ChIP-seq for MYC on these cell lines to determine whether we would also observe increased MYC occupancy at core promoters and enhancers of active genes and whether there would be saturation at the high affinity E-box sites as well within our specific cell type. Would the localization of MYC at the promoters of active genes correlate to our gene expression data? ChIP-seq could also address whether our system of exogenous MYC induction is

at such high levels that MYC is overwhelming the ability of HIFs to exert their activity upon MYC activity.

It would be quite valuable to generate an inducible system of MYC in which expression could be fine-tuned to not only control when it's activated but how much is activated. This would allow us to investigate whether low levels of MYC induction would yield similar or completely different gene expression results. It would also be invaluable to perform such efforts in other pVHL deficient RCC cell lines. Understanding the molecular interplay between MYC and HIFs within ccRCC would serve a means of uncovering potential vulnerabilities for targeted therapies.

Chapter 3 discussion and future directions

There is a vital need for GEM models that accurately recapitulate the molecular and histopathological features of human ccRCC. Significant work has been done over the years by several groups—including our own, to satisfy such a need. Our group has demonstrated that MYC overexpression within renal tubule cells gives rise to pRCC. Previous work from Shroff and colleagues also generated a mouse model that overexpressed MYC. However, their use of the gamma-glutamyl transferase promoter yielded tumors that were histologically consistent with collecting duct RCC (cdRCC)[147]. Such evidence strongly suggests that cell of origin may be just as crucial as genetic alterations in order to generate faithful models RCC.

Large-scale genomic analysis revealed that focal amplification of 8q24 (MYC) is found in 15% of ccRCC tumors while ~32% undergo a focal loss of 9p21 (CDKN2A) . Such evidence led us to generate the following cohorts of mice all the presence of *VHL* loss. *VM* mice harbor a combination of *VHL* loss and overexpression of *MYC* within

renal tubule cells and *VIM* mice harbor the combinatorial loss of VHL, germline deletion of Ink4a/Arf, and overexpression of MYC. We also generated a cohort of mice that only harbored inactivation of *VHL,* termed *V* mice. As expected, *V* mice had the greatest overall survival and did not develop tumors. However, *VM* and *VIM* mice experienced significantly worse overall survival, with *VIM* mice experiencing the worse overall survival out of all three cohorts. While *VM* mice did develop tumors at high penetrance of 67%, *VIM* mice had a 100% penetrance, were generally of a higher grade, displayed clear cell histology, and displayed some instances of liver metastases (~33%). It should be noted that while *VIM* tumors recapitulated some of the most characteristic features of ccRCC, there were some interesting observations within this model.

Metastases was only observed within the *VIM* cohort; albeit at a relatively low rate (Table 3.1). A previous study by Bianchi and colleagues assessed the distribution of various sites of metastases in patients with RCC and found the most common site to be the lung (45%)[173]. This was followed by bone (30%), lymph node (22%), and liver (20%) as the next most frequent sites of metastases among RCC patients. It should be noted that there was no sub-classification of the primary tumors other than cancer of kidney—so one cannot ascribe the frequency of metastases being attributable to a specific subtype of RCC. Nonetheless, while we did not see any metastases to the lung, it is possible that our model still represents a subset of RCC patients that do experience liver metastases.

Additionally, the upregulation of genes involved in promoting invasion and metastases through remodeling of the extracellular matrix (ECM) in *VIM* cell lines supports the metastatic phenotype observed in this model (Figure 3.5d). However, one

should note that such analysis was performed in one representative *VIM* cell line. It would be worth determining whether such findings would be supported in *VIM* primary tumors by looking at the gene expression data of the same genes. I would hypothesize that we would find similar results seeing as that tumors provide a more reliable depiction of the microenvironment compared to cell lines that are grown on plastic. Furthermore, is it possible that the aggressive nature of the *VIM* tumors were not specific to the inactivation of *Ink4a/Arf* in the kidney—but due to the systemic loss of *Ink4a/Arf*? It would be interesting to determine whether deletion of *Ink4a/Arf* within the kidney would yield the same aggressive phenotype. As such, GEM models are indispensable tools to better understand and investigate the complexities of disease. Our GEM models of RCC, while not perfect, contributes significantly to the field of cancer research.

REFERENCES

1. Siegel, R. L., Miller, K. D. & Jemal, A. Cancer statistics, 2019. *Ca Cancer J Clin* **69,** 7–34 (2019).

2. Hsieh, J. J. *et al.* Renal cell carcinoma. *Nat Rev Dis Primers* **3,** 17009 (2017).

3. Semenza, G. L. Hypoxia-inducible factors: mediators of cancer progression and targets for cancer therapy. *Trends Pharmacol Sci* **33,** 207–214 (2012).

4. Sato, Y. *et al.* Integrated molecular analysis of clear-cell renal cell carcinoma. *Nat Genet* **45,** 860–867 (2013).

5. Network, T. Comprehensive molecular characterization of clear cell renal cell carcinoma. *Nature* **499,** 43 (2013).

6. Beroukhim, R. *et al.* Patterns of Gene Expression and Copy-Number Alterations in von-Hippel Lindau Disease-Associated and Sporadic Clear Cell Carcinoma of the Kidney. *Cancer Res* **69,** 4674–4681 (2009).

7. Network, T. Comprehensive Molecular Characterization of Papillary Renal-Cell Carcinoma. *New Engl J Medicine* **374,** 135–145 (2016).

8. Furge, K. A. *et al.* Detection of DNA Copy Number Changes and Oncogenic Signaling Abnormalities from Gene Expression Data Reveals MYC Activation in High-Grade Papillary Renal Cell Carcinoma. *Cancer Res* **67,** 3171–3176 (2007).

9. Brunelli, M. *et al.* Eosinophilic and classic chromophobe renal cell carcinomas have similar frequent losses of multiple chromosomes from among chromosomes 1, 2, 6, 10, and 17, and this pattern of genetic abnormality is not present in renal oncocytoma. *Modern Pathol* **18,** 3800286 (2005).

10. Nickerson, M. L. *et al.* Mutations in a novel gene lead to kidney tumors, lung wall defects, and benign tumors of the hair follicle in patients with the Birt-Hogg-Dubé syndrome. *Cancer Cell* **2,** 157–164 (2002).

11. Shuch, B. *et al.* Germline PTEN Mutation Cowden Syndrome: An Underappreciated Form of Hereditary Kidney Cancer. *J Urology* **190,** 1990–1998 (2013).

12. Iliopoulos, O., Kibel, A., Gray, S. & Kaelin, W.
Tumour suppression by the human von Hippel-Lindau gene product. *Nature Medicine* **1,** (1995).

13. Schoenfeld, A., Davidowitz, E. J. & Burk, R. D. A second major native von Hippel–Lindau gene product, initiated from an internal translation start site, functions as a tumor suppressor. *Proc National Acad Sci* **95,** 8817–8822 (1998).

14. Iwai, K. *et al.* Identification of the von Hippel–Lindau tumor-suppressor protein as part of an active E3 ubiquitin ligase complex. *Proc National Acad Sci* **96,** 12436–12441 (1999).

15. Lisztwan, J., Imbert, G. & Krek, W. The von Hippel–Lindau tumor suppressor protein is a component of an E3 ubiquitin–protein ligase activity. *Genes and Development* **13,** 1822–1833 (1999).

16. Cockman, M. E. *et al.* Hypoxia inducible factor-alpha binding and ubiquitylation by the von Hippel-Lindau tumor suppressor protein. *J Biol Chem* **275,** 25733–25741 (2000).

17. Ohh, M. *et al.* Ubiquitination of hypoxia-inducible factor requires direct binding to the β-domain of the von Hippel–Lindau protein. *Nat Cell Biol* **2,** ncb0700_423 (2000).

18. Maxwell, P. H. *et al.* The tumour suppressor protein VHL targets hypoxia-inducible factors for oxygen-dependent proteolysis. *Nature* **399,** 271 (1999).

19. Bruick, R. K. & McKnight, S. L. A Conserved Family of Prolyl-4-Hydroxylases That Modify HIF. *Science* **294,** 1337–1340 (2001).

20. Min, J.-H. & Pavletich, N. P. Structure of and HIF-1a-pVHL Complex: Hydroxyproline Recognition in Signaling. *Science* **296,** 1886–1889 (2002).

21. Hon, W.-C., Wilson, M. I. & Jones, Y. E. Structural basis for the recognition of hydroxyproline in HIF-1 a by pVHL. *Nature* **417,** 975–978 (2002).

22. Kallio, P. J., Pongratz, I., Gradin, K., McGuire, J. & Poellinger, L. Activation of hypoxia-inducible factor 1α: Posttranscriptional regulation and conformational change by recruitment of the Arnt transcription factor. *Proc National Acad Sci* **94,** 5667–5672 (1997).

23. Salceda, S. & Caro, J. Hypoxia-inducible Factor 1a (HIF-1a) Protein Is Rapidly Degraded by the Ubiquitin-Proteasome System under Normoxic Conditions. *The Journal of Biological Chemistry* **272,** 22642–22647 (1997).

24. Beischlag, T. V. & Perdew, G. H. The Aryl Hydrocarbon Receptor Complex and the Control of Gene Expression. *Crit Rev Eukaryot Gene Expr* **18,** 207–250 (2008).

25. Wang, G. L., Jiang, B.-H. & Semenza, G. L. Hypoxia-inducible factor 1 is a basic-helix-loop-helix-PAS heterodimer regulated by cellular 02 tension. *PNAS* **92,** 5510–5514 (1995).

26. Wang, G. L. & Semenza, G. L. Purification and Characterization of Hypoxia-inducible Factor 1. *The Journal of Biological Chemistry* **270,** 1230–1237 (1995).

27. Li, H. & Whitlock, J. P. Induction of Phosphoglycerate Kinase 1 Gene Expression by Hypoxia. *The Journal of Biological Chemistry* **271,** 21262–21267 (1996).

28. Breen, M. E. & Mapp, A. K. Modulating the masters: chemical tools to dissect CBP and p300 function. *Curr Opin Chem Biol* **45,** 195–203 (2018).

29. Yamashita, K., Discher, D. J., Hu, J., Bishopric, N. H. & Webster, K. A. Molecular Regulation of the Endothelin-1 Gene by Hypoxia . *J Biol Chem* **276,** 12645–12653 (2001).

30. Krek, W. VHL takes HIF's breath away. *Nat Cell Biol* **2,** 121–123 (2000).

31. Ema, M. *et al.* A novel bHLH-PAS factor with close sequence similarity to hypoxia-inducible factor 1α regulates the VEGF expression and is potentially involved in lung and vascular development. *Proc National Acad Sci* **94,** 4273–4278 (1997).

32. Wiesener, M. S. & Jurgensen, J. Widespread, hypoxia-inducible expression of HIF-2 α in distinct cell populations of different organs. *The FASEB Journal* **17,** 271–273 (2002).

33. Makino, Y. & Poellinger, L. Inhibitory PAS domain protein is a negative regulator of hypoxia-inducible gene expression. *Nature* **414,** 550–554 (2001).

34. Kotch, L. E., Iyer, N. V., Laughner, E. & Semenza, G. L. Defective Vascularization of HIF-1α-Null Embryos Is Not Associated with VEGF Deficiency but with Mesenchymal Cell Death. *Dev Biol* **209,** 254–267 (1999).

35. Compernolle, V. *et al.* Loss of HIF-2α and inhibition of VEGF impair fetal lung maturation, whereas treatment with VEGF prevents fatal respiratory distress in premature mice. *Nat Med* **8,** 702 (2002).

36. Hu, C.-J., Sataur, A. & Simon, C. M. The N-Terminal Transactivation Domain Confers Target Gene Specificity of Hypoxia-inducible Factors HIF-1 and HIF-2. *Molecular Biology of the Cell* **18,** 4528–4542 (2007).

37. Hu, C.-J., Wang, L.-Y., Chodosh, L. A., Keith, B. & Simon, C. M. Differential Roles of Hypoxia-Inducible Factor 1α (HIF-1α) and HIF-2α in Hypoxic Gene Regulation. *Mol Cell Biol* **23,** 9361–9374 (2003).

38. Wang, V. & Yarchoan, R. Differential Gene Up-Regulation by Hypoxia-Inducible Factor-1 AA and Hypoxia-Inducible Factor-2 AA in HEK293T Cells. *Cancer Research* **65,** 3299–3306 (2005).

39. Covello, K. L. *et al.* HIF-2α regulates Oct-4: effects of hypoxia on stem cell function, embryonic development, and tumor growth. *Gene Dev* **20,** 557–570 (2006).

40. Baba, M. *et al.* Loss of von Hippel-Lindau protein causes cell density dependent deregulation of CyclinD1 expression through Hypoxia-inducible factor. *Oncogene* **22,** 2728 (2003).

41. Lando, D. *et al.* FIH-1 is an asparaginyl hydroxylase enzyme that regulates the transcriptional activity of hypoxia-inducible factor. *Gene Dev* **16,** 1466–1471 (2002).

42. Bracken, C. P. *et al.* Cell-specific Regulation of Hypoxia-inducible Factor (HIF)-1α and HIF-2α Stabilization and Transactivation in a Graded Oxygen Environment. *J Biol Chem* **281,** 22575–22585 (2006).

43. Vasavada, S. P., Novick, A. C. & Williams, B. p53, bcl-2, and Bax Expression in Renal Cell Carcinoma. *Urology* **51,** 1057–1061 (1998).

44. Sendoel, A., Kohler, I. & Hengartner, M. O. HIF-1 antagonizes p53-mediated apoptosis through a secreted neuronal tyrosinase. *Nature* **465,** 577–583 (2010).

45. Sánchez-Puig, N., Veprintsev, D. B. & Fersht, A. R. Binding of Natively Unfolded HIF-1α ODD Domain to p53. *Mol Cell* **17,** 11–21 (2005).

46. An, W. G., Kanekal, M. & Neckers, L. M. Stabilization of wild-type p53 by hypoxia-inducible factor 1 a. *Nature* **392,** 405–407 (1998).

47. Roe, J.-S. *et al.* p53 Stabilization and Transactivation by a von Hippel-Lindau Protein. *Mol Cell* **22,** 395–405 (2006).

48. Clark, P. E. The role of VHL in clear-cell renal cell carcinoma and its relation to targeted therapy. *Kidney Int* **76,** 939–945 (2009).

49. Rini, B. I. & kins, M. Resistance to targeted therapy in renal-cell carcinoma. *Lancet Oncol* **10,** 992–1000 (2009).

50. Motzer, R. J. *et al.* Nivolumab versus Everolimus in Advanced Renal-Cell Carcinoma. *New Engl J Medicine* **373,** 1803–1813 (2015).

51. Herman, J. *et al.* Silencing of the VHL tumor-suppressor gene by DNA methylation in renal carcinoma. *Proc National Acad Sci* **91,** 9700–9704 (1994).

52. Gnarra, J. R. *et al.* Defective placental vasculogenesis causes embryonic lethality in VHL-deficient mice. *Proc National Acad Sci* **94,** 9102–9107 (1997).

53. Ma, W., Tessarollo, L., Hong, S.-B., Zbar, B. & Schmidt, L. S. Hepatic Vascular Tumors, Angiectasis in Multiple Organs, and Impaired Spermatogenesis in Mice with Conditional Inactivation of the VHL Gene. *Cancer Research* **63,** 5320–5328 (2003).

54. Haase, V. H., Glickman, J. N., Socolovsky, M. & Jaenisch, R. Vascular tumors in livers with targeted inactivation of the von Hippel–Lindau tumor suppressor. *Proc National Acad Sci* **98,** 1583–1588 (2001).

55. Kleymenova, E. *et al.* Susceptibility to vascular neoplasms but no increased susceptibility to renal carcinogenesis in Vhl knockout mice. *Carcinogenesis* **25,** 309–315 (2004).

56. Lonser, R. R. *et al.* von Hippel-Lindau disease. *Lancet* **361,** 2059–2067 (2003).

57. Rankin, E. B., Tomaszewski, J. E. & Haase, V. H. Renal Cyst Development in Mice with Conditional Inactivation of the von Hippel-Lindau Tumor Suppressor. *Cancer Res* **66,** 2576–2583 (2006).

58. Frew, I. J. & Moch, H. A Clearer View of the Molecular Complexity of Clear Cell Renal Cell Carcinoma. *Annu Rev Pathology Mech Dis* **10,** 1–27 (2015).

59. Frew, I. J. *et al.* pVHL and PTEN tumour suppressor proteins cooperatively suppress kidney cyst formation. *Embo J* **27,** 1747–1757 (2008).

60. Pritchett, T., Bader, H., Henderson, J. & Hsu, T. Conditional inactivation of the mouse von Hippel–Lindau tumor suppressor gene results in wide-spread hyperplastic, inflammatory and fibrotic lesions in the kidney. *Oncogene* **34,** 2631 (2015).

61. Velickovic, M., B.Sc, Delahunt & Grebe, K. Intragenic PTEN/MMAC1 Loss of Heterozygosity in Conventional (Clear-Cell) Renal Cell Carcinoma is Associated with Poor Patient Prognosis. *Mod Pathol* **15,** 479–485 (2002).

62. Hollander, C. M., Blumenthal, G. M. & Dennis, P. A. PTEN loss in the continuum of common cancers, rare syndromes and mouse models. *Nat Rev Cancer* **11,** 289 (2011).

63. Hollstein, M., Sidransk, D. & Harris, C. C. p53 Mutations in Human Cancers. *Science* **253,** 49–53 (1991).

64. Kandoth, C. *et al.* Mutational landscape and significance across 12 major cancer types. *Nature* **502,** 333 (2013).

65. Brosh, R. & Rotter, V. When mutants gain new powers: news from the mutant p53 field. *Nat Rev Cancer* **9,** 701–713 (2009).

66. Albers, J. *et al.* Combined mutation of Vhl and Trp53 causes renal cysts and tumours in mice. *Embo Mol Med* **5,** 949–964 (2013).

67. Yoder, B. K. Role of Primary Cilia in the Pathogenesis of Polycystic Kidney Disease. *J Am Soc Nephrol* **18,** 1381–1388 (2007).

68. Hergovich, A., Lisztwan, J., Barry, R., Ballschmieter, P. & Krek, W. Regulation of microtubule stability by the von Hippel-Lindau tumour suppressor protein pVHL. *Nat Cell Biol* **5,** ncb899 (2002).

69. Berbari, N. F., O'Connor, A. K., Haycraft, C. J. & Yoder, B. K. The Primary Cilium as a Complex Signaling Center. *Curr Biol* **19,** R526–R535 (2009).

70. Lehmann, H., Vicari, D., Wild, P. J. & Frew, I. J. Combined Deletion of Vhl and Kif3a Accelerates Renal Cyst Formation. *J Am Soc Nephrol* **26,** 2778–2788 (2015).

71. Harlander, S. *et al.* Combined mutation in Vhl, Trp53 and Rb1 causes clear cell renal cell carcinoma in mice. *Nat Med* **23,** 869–877 (2017).

72. Genega, E. M. *et al.* Carbonic Anhydrase IX Expression in Renal NeoplasmsCorrelation With Tumor Type and Grade. *Am J Clin Pathol* **134,** 873–879 (2010).

73. Duns, G. *et al.* Histone Methyltransferase Gene SETD2 Is a Novel Tumor Suppressor Gene in Clear Cell Renal Cell Carcinoma. *Cancer Res* **70,** 4287–4291 (2010).

74. Peña-Llopis, S. *et al.* BAP1 loss defines a new class of renal cell carcinoma. *Nat Genet* **44,** 751 (2012).

75. Varela, I. *et al.* Exome sequencing identifies frequent mutation of the SWI/SNF complex gene PBRM1 in renal carcinoma. *Nature* **469,** 539 (2011).

76. Jensen, D. E. *et al.* BAP1: a novel ubiquitin hydrolase which binds to the BRCA1 RING finger and enhances BRCA1-mediated cell growth suppression. *Oncogene* **16,** 1201861 (1998).

77. Ventii, K. H. *et al.* BRCA1-Associated Protein-1 Is a Tumor Suppressor that Requires Deubiquitinating Activity and Nuclear Localization. *Cancer Res* **68,** 6953–6962 (2008).

78. Wang, S.-S. *et al.* Bap1 is essential for kidney function and cooperates with Vhl in renal tumorigenesis. *Proc National Acad Sci* **111,** 16538–16543 (2014).

79. Gu, Y.-F. *et al.* Modeling Renal Cell Carcinoma in Mice: Bap1 and Pbrm1 Inactivation Drive Tumor Grade. *Cancer Discov* **7,** 900–917 (2017).

80. Sharma, R., Sanchez-Ferras, O. & Bouchard, M. Pax genes in renal development, disease and regeneration. *Semin Cell Dev Biol* **44,** 97–106 (2015).

81. Nargund, A. M. *et al.* The SWI/SNF Protein PBRM1 Restrains VHL-Loss-Driven Clear Cell Renal Cell Carcinoma. *Cell Reports* **18,** 2893–2906 (2017).

82. Kapur, P. *et al.* Effects on survival of BAP1 and PBRM1 mutations in sporadic clear-cell renal-cell carcinoma: a retrospective analysis with independent validation. *Lancet Oncol* **14,** 159–167 (2013).

83. Farrell, A. S. & Sears, R. C. MYC Degradation. *Csh Perspect Med* **4,** a014365 (2014).

84. Duesberg, P., Bister, K. & Vogt, P. The RNA of avian acute leukemia virus MC29. *Proc National Acad Sci* **74,** 4320–4324 (1977).

85. Neel, B., Jhanwar, S., Chaganti, R. & Hayward, W. Two human c-onc genes are located on the long arm of chromosome 8. *Proc National Acad Sci* **79,** 7842–7846 (1982).

86. Dalla-Favera, R. & Croce, C. M. Human c-myc onc gene is located on the region of chromosome 8 that is translocated in Burkitt lymphoma cells. *Proc Natl Acad Sci* **79,** 7824–7827 (1982).

87. Nikiforov, M. A. *et al.* A Functional Screen for Myc-Responsive Genes Reveals Serine Hydroxymethyltransferase, a Major Source of the One-Carbon Unit for Cell Metabolism. *Mol Cell Biol* **22,** 5793–5800 (2002).

88. Kim, H. *et al.* HuR recruits let-7/RISC to repress c-Myc expression. *Gene Dev* **23,** 1743–1748 (2009).

89. Sampson, V. B. *et al.* MicroRNA Let-7a Down-regulates MYC and Reverts MYC-Induced Growth in Burkitt Lymphoma Cells. *Cancer Res* **67,** 9762–9770 (2007).

90. Lal, A., Navarro, F. & Lieberman, J. miR-24 inhibits cell proliferation by suppressing expression of E2F2, MYC and other cell cycle regulatory genes by binding to “seedless” 3 ′ UTR microRNA recognition elements. **35,** 610–625 (2009).

91. Wall, M., Poortinga, G. & McArthur, G. A. Translational control of c-MYC by rapamycin promotes terminal myeloid differentiation. *Blood* **112,** 2305–2317 (2008).

92. Tseng, Y.-Y. *et al.* PVT1 dependence in cancer with MYC copy-number increase. *Nature* **512,** 82 (2014).

93. Sears, R., Leone, G., DeGregori, J. & Nevins, J. R. Ras Enhances Myc Protein Stability. *Mol Cell* **3,** 169–179 (1999).

94. Sears, R. *et al.* Multiple Ras-dependent phosphorylation pathways regulate Myc protein stability. *Gene Dev* **14,** 2501–2514 (2000).

95. Magudia, K., Lahoz, A. & Hall, A. K-Ras and B-Raf oncogenes inhibit colon

epithelial polarity establishment through up-regulation of c-myc. *J Cell Biology* **198,** 185–194 (2012).

96. Hung, C.-L. *et al.* A long noncoding RNA connects c-Myc to tumor metabolism. *Proc National Acad Sci* **111,** 18697–18702 (2014).

97. Roussel, M. F., Cleveland, J. L. & Sherr, C. J. Myc rescue of a mutant CSF-1 receptor impaired in mitogenic signalling. *Nature* **353,** 361–363 (1991).

98. Bowman, T. *et al.* Stat3-mediated Myc expression is required for Src transformation and PDGF-induced mitogenesis. *Proc National Acad Sci* **98,** 7319–7324 (2001).

99. Barone, V. M. & Courtneidge, S. A. Myc but not Fos rescue of PDGF signalling block caused by kinase-inactive Src. *Nature* **378,** 509–512 (1995).

100. Lau, L. & Nathans, D. Expression of a set of growth-related immediate early genes in BALB/c 3T3 cells: coordinate regulation with c-fos or c-myc. *Proc National Acad Sci* **84,** 1182–1186 (1987).

101. Palomero, T., Lim, W. & Ferrando, A. A. NOTCH1 directly regulates c-MYC and activates a feed-forward-loop transcriptional network promoting leukemic cell growth. *PNAS* **104,** 18261–18266 (2007).

102. Weng, A. P. *et al.* c-Myc is an important direct target of Notch1 in T-cell acute lymphoblastic leukemia/lymphoma. *Gene Dev* **20,** 2096–2109 (2006).

103. Chou, Y.-T. *et al.* EGFR Promotes Lung Tumorigenesis by Activating miR-7 through a Ras/ERK/Myc Pathway That Targets the Ets2 Transcriptional Repressor ERF. *Cancer Res* **70,** 8822–8831 (2010).

104. Conacci-Sorrell, M., McFerrin, L. & Eisenman, R. N. An Overview of MYC and Its Interactome. *Csh Perspect Med* **4,** a014357 (2014).

105. Yashiro-Ohtani, Y. *et al.* Long-range enhancer activity determines Myc sensitivity to Notch inhibitors in T cell leukemia. *Proc National Acad Sci* **111,** E4946–E4953 (2014).

106. Herranz, D. *et al.* A NOTCH1-driven MYC enhancer promotes T cell development, transformation and acute lymphoblastic leukemia. *Nat Med* **20,** nm.3665 (2014).

107. Grisanzio, C. & Freedman, M. L. Chromosome 8q24–Associated Cancers and MYC. *Genes Cancer* **1,** 555–559 (2010).

108. Ahmadiyeh, N. *et al.* 8q24 prostate, breast, and colon cancer risk loci show tissue-specific long-range interaction with MYC. *Proc National Acad Sci* **107,** 9742–9746 (2010).

109. Yochum, G. S., Sherrick, C. M., MacPartlin, M. & Goodman, R. H. A β-catenin/TCF-coordinated chromatin loop at MYC integrates 5′ and 3′ Wnt responsive enhancers. *Proc National Acad Sci* **107,** 145–150 (2010).

110. Zanet, J. *et al.* Endogenous Myc controls mammalian epidermal cell size, hyperproliferation, endoreplication and stem cell amplification. *J Cell Sci* **118,** 1693–1704 (2005).

111. Sansom, O. J. *et al.* Myc deletion rescues Apc deficiency in the small intestine. *Nature* **446,** 676 (2007).

112. Wang, R. *et al.* The Transcription Factor Myc Controls Metabolic Reprogramming upon T Lymphocyte Activation. *Immunity* **35,** 871–882 (2011).

113. Klatte, T. *et al.* Gain of chromosome 8q is associated with metastases and poor survival of patients with clear cell renal cell carcinoma. *Cancer* **118,** 5777–5782 (2012).

114. Gil, J. & Peters, G. Regulation of the INK4b–ARF–INK4a tumour suppressor locus: all for one or one for all. *Nat Rev Mol Cell Bio* **7,** nrm1987 (2006).

115. Modesto, M. & Quelle, D. E. The Alternative Reading Frame Tumor Suppressor Inhibits Growth through p21-dependent and p21-independent Pathways. *Cancer Research* **61,** 3145–3150 (2001).

116. Weber, J. D. *et al.* p53-independent functions of the p19ARF tumor suppressor. *Gene Dev* **14,** 2358–2365 (2000).

117. Latres, E. & Barbacid, M. Limited overlapping roles of P15 INK4b and P18 INK4c cell cycle inhibitors in proliferation and tumorigenesis. *The EMBO Journal* **19,** 3496–3506 (2000).

118. Sharpless, N. E., Ramsey, M. R., Balasubramanian, P., Castrillon, D. H. & DePinho, R. A. The differential impact of p16INK4a or p19ARF deficiency on cell growth and tumorigenesis. *Oncogene* **23,** 1207074 (2004).

119. Schullerus, D. & Kovacs, G. Loss of heterozygosity at chromosomes 8p, 9p, and 14q is associated with stage and grade of non-papillary renal cell carcinomas. *Journal of Pathology* **183,** 151–155 (1997).

120. Grady, B. & Dahiya, R. Frequently deleted loci on chromosome 9 may harbor several tumor suppressor genes in human renal cell carcinoma. *J Urology* **166,** 1088–1092 (2001).

121. El-Mokadem, I. *et al.* Chromosome 9p deletion in clear cell renal cell carcinoma predicts recurrence and survival following surgery. *Brit J Cancer* **111,** 1381 (2014).

122. Kawada, Y. *et al.* Aberrations of the p14ARF and p16INK4a Genes in Renal Cell Carcinomas. *Jpn J Cancer Res* **92,** 1293–1299 (2001).

123. Ikuerowo, S. O. *et al.* p16INK4a Expression and Clinicopathologic Parameters in Renal Cell Carcinoma. *Eur Urol* **51,** 732–738 (2007).

124. Kondo, K., Klco, J., Nakamura, E., Lechpammer, M. & Kaelin, W. G. Inhibition of HIF is necessary for tumor suppression by the von Hippel-Lindau protein. *Cancer Cell* **1,** 237–246 (2002).

125. Kondo, K., Kim, W. Y., Lechpammer, M. & Kaelin, W. G. Inhibition of HIF2α Is Sufficient to Suppress pVHL-Defective Tumor Growth. *Plos Biol* **1,** e83 (2003).

126. Raval, R. R., Lau, K., Tran, M. G. & Ratcliffe, P. J. Contrasting Properties of Hypoxia-Inducible Factor 1 (HIF-1) and HIF-2 in von Hippel-Lindau-Associated Renal Cell Carcinoma. *Molecular and Cellular Biology* **25,** 5675–5686 (2005).

127. Maranchie, J. K. *et al.* The contribution of VHL substrate binding and HIF1-α to the phenotype of VHL loss in renal cell carcinoma. *Cancer Cell* **1,** 247–255 (2002).

128. Gardner, L. B. *et al.* Hypoxia inhibits G1/S transition through regulation of p27 expression. *J Biol Chem* **276,** 7919–7926 (2001).

129. Goda, N. & Johnson, R. S. Hypoxia-Inducible Factor 1 Is Essential for Cell Cycle Arrest during Hypoxia. *Molecular and Cellular Biology* **23,** 359–369 (2003).

130. GREEN, S. L. & GIACCIA, A. J. p21Cip1 and p27Kip1 Regulate Cell Cycle Reentry after Hypoxic Stress but Are Not Necessary for Hypoxia-Induced Arrest. *Molecular and Cellular Biology* **21,** 1196–1206 (2001).

131. Koshiji, M. *et al.* HIF-1α induces cell cycle arrest by functionally counteracting Myc. *Embo J* **23,** 1949–1956 (2004).

132. Koshiji, M. *et al.* HIF-1α Induces Genetic Instability by Transcriptionally Downregulating MutSα Expression. *Mol Cell* **17,** 793–803 (2005).

133. Mack, F. A. & Simon, C. M. Decreased Growth of Vhl-/- Fibrosarcomas Is Associated with Elevated Levels of Cyclin Kinase Inhibitors p21 and p27. *Molecular and Cellular Biology* **25,** 4565–4578 (2005).

134. Gordan, J. D., Bertout, J. A., Hu, C.-J., Diehl, A. J. & Simon, C. M. HIF-2α Promotes Hypoxic Cell Proliferation by Enhancing c-Myc Transcriptional Activity. *Cancer Cell* **11,** 335–347 (2007).

135. Gordan, J. D. *et al.* HIF-α Effects on c-Myc Distinguish Two Subtypes of Sporadic

VHL-Deficient Clear Cell Renal Carcinoma. *Cancer Cell* **14,** 435–446 (2008).

136. Brodaczewska, K. K., Szczylik, C., Fiedorowicz, M., Porta, C. & Czarnecka, A. M. Choosing the right cell line for renal cell cancer research. *Mol Cancer* **15,** 83 (2016).

137. Bailey, S. T. *et al.* MYC activation cooperates with Vhl and Ink4a/Arf loss to induce clear cell renal cell carcinoma. *Nat Commun* **8,** ncomms15770 (2017).

138. Siegel, R., Ma, J., Zou, Z. & Jemal, A. Cancer statistics, 2014. *Ca Cancer J Clin* **64,** 9–29 (2014).

139. Linehan, M. W. *et al.* Genetic Basis of Cancer of the Kidney Disease-Specific Approaches to Therapy. *Clinical Cancer Research* **10,** 6282–6289 (2004).

140. Kim, W. Y. & Kaelin, W. G. Role of VHL Gene Mutation in Human Cancer. *J Clin Oncol* **22,** 4991–5004 (2004).

141. Brugarolas, J. Molecular Genetics of Clear-Cell Renal Cell Carcinoma. *J Clin Oncol* **32,** 1968–1976 (2014).

142. Davis, C. F. *et al.* The Somatic Genomic Landscape of Chromophobe Renal Cell Carcinoma. *Cancer Cell* **26,** 319–330 (2014).

143. Shen, C. & Kaelin, W. G. The VHL/HIF axis in clear cell renal carcinoma. *Semin Cancer Biol* **23,** 18–25 (2013).

144. Zimmer, M., Doucette, D., Siddiqu, N. & Iliopoulos, O. Inhibition of Hypoxia-Inducible Factor Is Sufficient for Growth Suppression of VHL–/– Tumors. *Molecular Cancer Research* **2,** 89–95 (2004).

145. Shen, C. *et al.* Genetic and Functional Studies Implicate HIF1α as a 14q Kidney Cancer Suppressor Gene. *Cancer Discov* **1,** 222–235 (2011).

146. Monzon, F. A. *et al.* Chromosome 14q loss defines a molecular subtype of clear-cell renal cell carcinoma associated with poor prognosis. *Modern Pathol* **24,** 1470 (2011).

147. Shroff, E. H. *et al.* MYC oncogene overexpression drives renal cell carcinoma in a mouse model through glutamine metabolism. *Proc National Acad Sci* **112,** 6539–6544 (2015).

148. Durinck, S. *et al.* Spectrum of diverse genomic alterations define non–clear cell renal carcinoma subtypes. *Nat Genet* **47,** ng.3146 (2014).

149. Serrano, M. *et al.* Role of the INK4a Locus in Tumor Suppression and Cell Mortality. *Cell* **85,** 27–37 (1996).

150. Erler, J. T. *et al.* Hypoxia-Induced Lysyl Oxidase Is a Critical Mediator of Bone Marrow Cell Recruitment to Form the Premetastatic Niche. *Cancer Cell* **15,** 35–44 (2009).

151. Erler, J. T. *et al.* Lysyl oxidase is essential for hypoxia-induced metastasis. *Nature* **440,** 1222 (2006).

152. Erler, J. T. & Giaccia, A. J. Lysyl Oxidase Mediates Hypoxic Control of Metastasis. *Cancer Res* **66,** 10238–10241 (2006).

153. Hiraga, T., Ito, S. & Nakamura, H. Cancer Stem–like Cell Marker CD44 Promotes Bone Metastases by Enhancing Tumorigenicity, Cell Motility, and Hyaluronan Production. *Cancer Res* **73,** 4112–4122 (2013).

154. Götte, M. & Yip, G. W. Heparanase, Hyaluronan, and CD44 in Cancers: A Breast Carcinoma Perspective. *Cancer Res* **66,** 10233–10237 (2006).

155. Kwon, M. & Berns, A. Mouse models for lung cancer. *Mol Oncol* **7,** 165–177 (2013).

156. Hezel, A. F., Kimmelman, A. C., Stanger, B. Z., Bardeesy, N. & DePinho, R. A. Genetics and biology of pancreatic ductal adenocarcinoma. *Gene Dev* **20,** 1218–1249 (2006).

157. Gan, B. *et al.* FoxOs Enforce a Progression Checkpoint to Constrain mTORC1-Activated Renal Tumorigenesis. *Cancer Cell* **18,** 472–484 (2010).

158. Baba, M. *et al.* Kidney-Targeted Birt-Hogg-Dubé Gene Inactivation in a Mouse Model: Erk1/2 and Akt-mTOR Activation, Cell Hyperproliferation, and Polycystic Kidneys. *Jnci J National Cancer Inst* **100,** 140–154 (2008).

159. Hasumi, Y. *et al.* Homozygous loss of BHD causes early embryonic lethality and kidney tumor development with activation of mTORC1 and mTORC2. *Proc National Acad Sci* **106,** 18722–18727 (2009).

160. Pollard, P. J. *et al.* Targeted Inactivation of Fh1 Causes Proliferative Renal Cyst Development and Activation of the Hypoxia Pathway. *Cancer Cell* **11,** 311–319 (2007).

161. Chen, J. *et al.* Deficiency of FLCN in Mouse Kidney Led to Development of Polycystic Kidneys and Renal Neoplasia. *Plos One* **3,** e3581 (2008).

162. David, K. A., Milowsky, M. I. & Nanus, D. M. Chemotherapy for Non–Clear-Cell Renal Cell Carcinoma. *Clin Genitourin Canc* **4,** 263–268 (2006).

163. Ivan, M. *et al.* Biochemical purification and pharmacological inhibition of a

mammalian prolyl hydroxylase acting on hypoxia-inducible factor. *Proc National Acad Sci* **99,** 13459–13464 (2002).

164. Gordan, J. D., Thompson, C. B. & Simon, C. M. HIF and c-Myc: sibling rivals for control of cancer cell metabolism and proliferation. *Cancer Cell* **12,** 108–113 (2007).

165. Kim, W. Y. & Sharpless, N. E. The Regulation of INK4/ARF in Cancer and Aging. *Cell* **127,** 265–275 (2006).

166. Linardopoulos, S. & Balmain, A. Deletion and Altered Regulation of p16INK4a and p15INK4b in Undifferentiated Mouse Skin Tumors. *Cancer Research* **55,** 5168–5172 (1995).

167. Chen, S. *et al.* Genome-wide CRISPR Screen in a Mouse Model of Tumor Growth and Metastasis. *Cell* **160,** 1246–1260 (2015).

168. Leeuwen, I. S. *et al.* Transgenic mice expressing tamoxifen-inducible Cre for somatic gene modification in renal epithelial cells. *Genesis* **44,** 225–232 (2006).

169. Liu, X. *et al.* ROCK Inhibitor and Feeder Cells Induce the Conditional Reprogramming of Epithelial Cells. *Am J Pathology* **180,** 599–607 (2012).

170. Wang, K. *et al.* MapSplice: Accurate mapping of RNA-seq reads for splice junction discovery. *Nucleic Acids Res* **38,** e178–e178 (2010).

171. Li, B. & Dewey, C. N. RSEM: accurate transcript quantification from RNA-Seq data with or without a reference genome. *BMC Bioinformatics* (2011).

172. Bullard, J. H., Purdom, E., Hansen, K. D. & Dudoit, S. Evaluation of statistical methods for normalization and differential expression in mRNA-Seq experiments. *Bmc Bioinformatics* **11,** 94 (2010).

173. Bianchi, M. *et al.* Distribution of metastatic sites in renal cell carcinoma: a population-based analysis. *Ann Oncol* **23,** 973–980 (2012).